VELOCITY STRUCTURE OF A METHANE HYDRATE STABILITY ZONE, OFFSHORE VANCOUVER ISLAND

Jacob French

Submitted in Partial Fulfillment of the Requirements
for the Degree of Bachelor of Science, Honours
Department of Earth Sciences
Dalhousie University, Halifax, Nova Scotia
March 1998

Distribution License

DalSpace requires agreement to this non-exclusive distribution license before your item can appear on DalSpace.

NON-EXCLUSIVE DISTRIBUTION LICENSE

You (the author(s) or copyright owner) grant to Dalhousie University the non-exclusive right to reproduce and distribute your submission worldwide in any medium.

You agree that Dalhousie University may, without changing the content, reformat the submission for the purpose of preservation.

You also agree that Dalhousie University may keep more than one copy of this submission for purposes of security, back-up and preservation.

You agree that the submission is your original work, and that you have the right to grant the rights contained in this license. You also agree that your submission does not, to the best of your knowledge, infringe upon anyone's copyright.

If the submission contains material for which you do not hold copyright, you agree that you have obtained the unrestricted permission of the copyright owner to grant Dalhousie University the rights required by this license, and that such third-party owned material is clearly identified and acknowledged within the text or content of the submission.

If the submission is based upon work that has been sponsored or supported by an agency or organization other than Dalhousie University, you assert that you have fulfilled any right of review or other obligations required by such contract or agreement.

Dalhousie University will clearly identify your name(s) as the author(s) or owner(s) of the submission, and will not make any alteration to the content of the files that you have submitted.

If you have questions regarding this license please contact the repository manager at dalspace@dal.ca.

Grant the distribution license by signing and dating below.

_____ _____

Name of signatory Date

Dalhousie University

Department of Earth Sciences
Halifax, Nova Scotia
Canada B3H 3J5
(902) 494-2358
FAX (902) 494-6889

DATE 16 Mar. 98

AUTHOR Jacob French

TITLE VELOCITY STRUCTURE OF A METHANE HYDRATE STABILITY ZONE, OFFSHORE VANCOUVER ISLAND

Degree H. BSc Convocation May Year 1998

Permission is herewith granted to Dalhousie University to circulate and to have copied for non-commercial purposes, at its discretion, the above title upon the request of individuals or institutions.

Abstract

The occurrence of methane hydrates within marine sediments of the accretionary prism of the Cascadia Margin, offshore Vancouver Island has been inferred by the occurrence of a bottom simulating reflector (BSR), which is believed to mark the phase boundary between methane hydrate and methane gas. A seismic study in May 1997 was undertaken in order to use wide-angle seismic data, with deployment of ocean bottom seismometers (OBSs), to model velocity-depth gradients within the methane hydrate stability zone. Wide-angle seismic data from a single OBS station is analyzed from 40 cu. in. and 300 cu. in. airgun sources along one line (Line 1) along a ridge structure where a strong BSR is known to occur. Velocity-depth modelling of the hydrate zone consists of 2 stages: 1) forward modelling of the layers to fit travel-time curves based on the given reflectors from the 40 cu. in. airgun source, and 2) using reflected and refracted phase arrivals from the 300 cu. in. airgun source to constrain the velocity gradients. The BSR displays variability with source frequency, with discontinuities in the BSR at vertical incidence observed with the higher frequency airgun data. The proposed model infers a low velocity gradient to depths slightly above the BSR, and a thin zone of high velocities (~32 m) directly above the BSR ranging from 1.79 to 1.86 km/s, which has a higher amount of hydrate concentration (~15-20%). Existence of a relatively thin layer of free gas (~22 m) with low velocities (~1.65 km/s) is postulated to exist below the BSR based on a strong reflector which occurs below BSR depths that might represent the base of the free-gas zone. The velocity models proposed support the proposition that the relative strength of the BSR might be the result of more than the amount of hydrate concentration within the methane hydrate stability field; instead, the continuity and strength of the reflector may be more closely linked to the nature of the underlying free gas zone.

Keywords: methane hydrates, BSR, Cascadia Margin, wide-angle seismics, velocity modelling

TABLE OF CONTENTS

TABLE OF FIGURES

TABLE OF TABLES

Acknowledgements

First and foremōst, I would like to thank my supervisor, Dr. Keith Louden, for this opportunity to dive in to hands-on seismic research, and without whose personal sacrifice and patience with this project, I would never have made it this far. To the rest of the Seismic Group, namely Thomas Funck, Deping Chian, and Bruce Mitchell: your patience is overwhelming. Keep up the good work. I would also like to acknowledge the Pacific Geoscience Centre and University of Victoria ship scientists for making the collection of data in this particular location possible. Many thanks to fellow students in the Earth Sciences Department who made it through this year and helped push me along.

CHAPTER 1 INTRODUCTION

1.1 Definition of methane hydrates

Methane hydrates (or methane clathrates) are naturally occurring solids in which molecules of natural gas, mainly methane, are trapped in a lattice framework of water molecules (Sloan, 1990). These methane hydrates are known to occur within marine sediments of continental slopes in a number of areas around the world, most notably in subduction zones where large accretionary sedimentary prisms have formed. The methane hydrate stability zone is limited to the upper sediment section (~300 metres below sea floor), below which temperatures are too high for hydrate to exist. Methane hydrate reservoirs may have significant economic importance, as they are undoubtedly the largest global source of natural gas (Kvenvolden, 1988; MacDonald, 1990). Because methane is a greenhouse gas, these methane hydrate reservoirs may also be influential in the global climate system (Kvenvolden, 1988). The magnitude of these hydrates is debatable, as accurate estimation requires improved knowledge of actual hydrate distribution in marine sediments (Korenaga et al., 1997). One crucial question is how continuous these methane hydrates are on a regional scale, and if their distribution can be inferred from seismic velocity-modelling studies.

1.2 Thesis Objective

The purpose of this project is to analyze the velocity structure of a methane hydrate zone of the Cascadia Margin (Fig. 1.1, Fig. 1.2) near Ocean Drilling Program (ODP) Site 889 (offshore Vancouver Island) using wide-angle seismic data. Seismic modelling will primarily involve velocity-depth analysis by forward modelling of wide-angle reflection and refraction data which allows the *P*-wave velocity distribution of the

a)

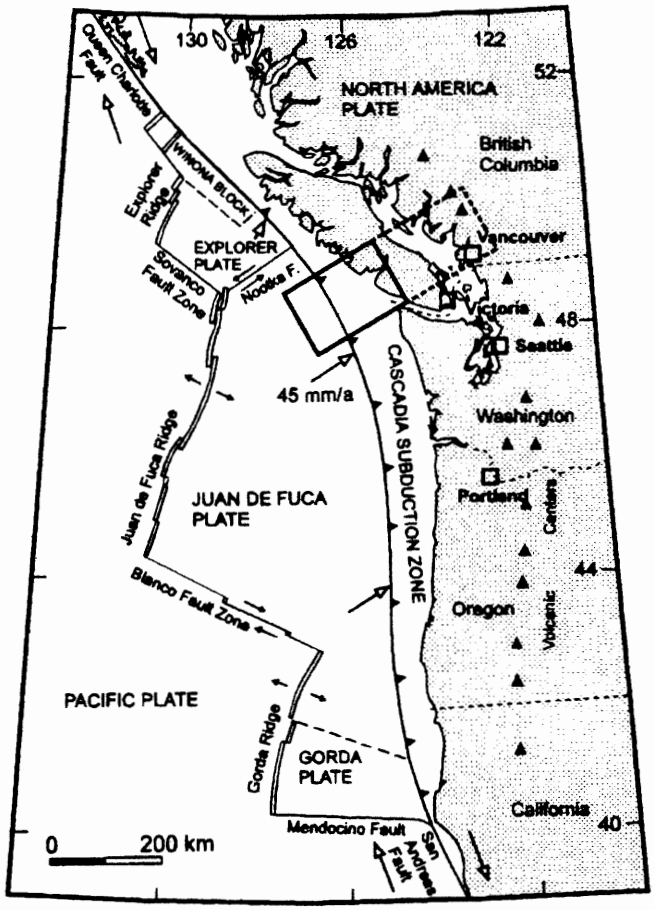

b)

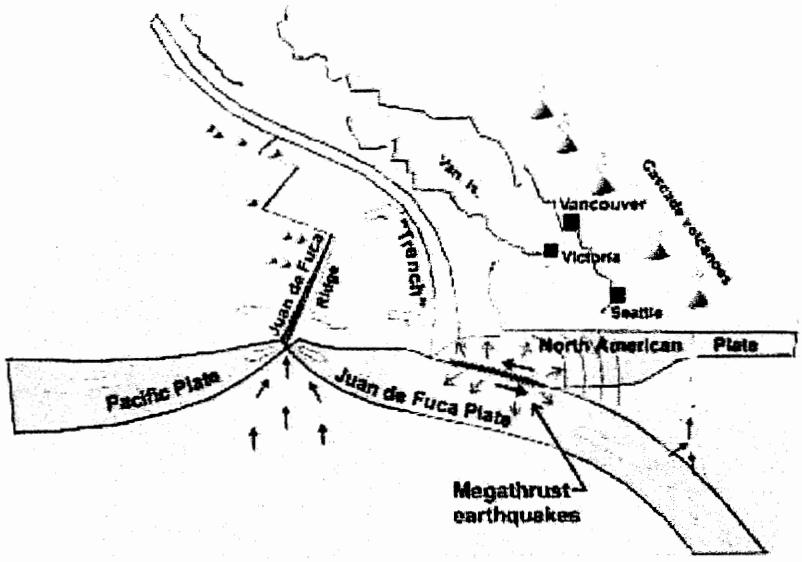

Figure 1.1 a) The Cascadia Margin and Juan de Fuca plate regime. The solid-line box outlines the offshore portion of the Lithoprobe transect. b) Cross-sectional view of the Cascadia Margin and Juan de Fuca plate regime. (From Hyndman, 1995)

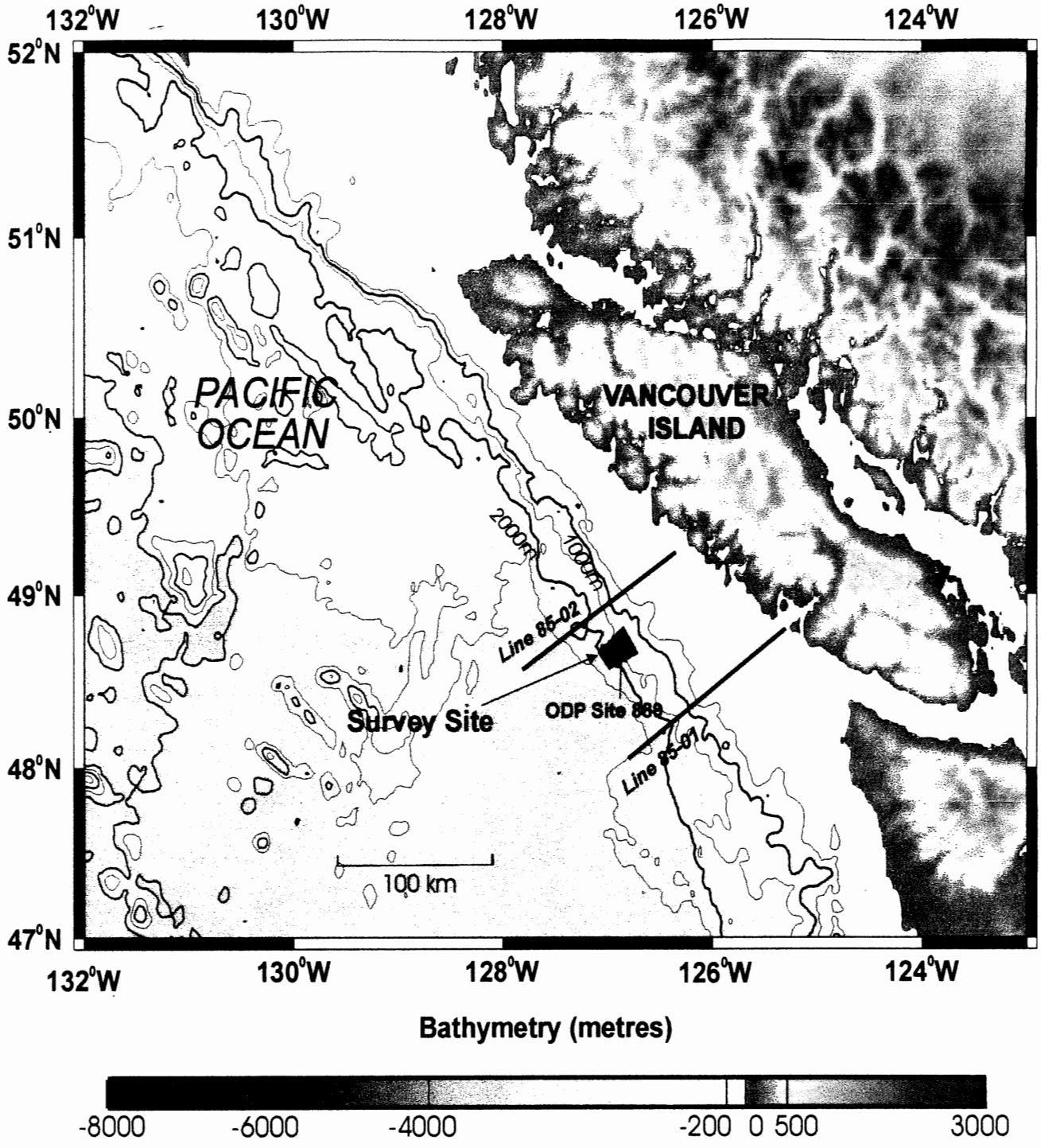

Figure 1.2. Bathymetry map of Vancouver Island Margin showing area of survey site (ODP Site 889) and location of LITHOPROBE multichannel seismic lines 85-01and 85-02.

sediment within and below the methane hydrate stability zone to be estimated. From these velocities, the physical properties of the sediments may then be inferred, followed by discussion of (1) how the velocity models compare with previous velocity models and drilling results, (2) the amount and concentration of both hydrate and free gas present, and (3) the characterization of the methane hydrates from wide-angle seismic profiles. The distribution of methane hydrates of the Cascadia Margin on a regional scale will then be discussed based on these analyses.

1.3 Tectonic and geological setting

1.3.1 Geology

The Cascadia Margin (Fig. 1.1a., Fig1.1b.) has been a zone of convergent plate motion since the Eocene. In recent times, the Juan de Fuca plate is being obliquely subducted beneath the North American plate (Riddihough, 1984; Duncan and Kulm, 1989; DeMets et al., 1990) which has led to the accretion of several terranes to the continent, namely the Crescent and Pacific Rim terranes (Vancouver Island and Olympic Peninsula).

The Vancouver Island Margin is composed of four tectonic units. The island itself (Wrangellia Terrane) was accreted to the North American Plate before the Late Cretaceous (Monger et al., 1982; Howell et al., 1985). The Pacific Rim Terrane just to the west is composed of Mesozoic sedimentary rocks wedged between the continent and ophiolites of the Crescent Terrane (Hyndman, 1995) (Fig 1.3). This Crescent Terrane is composed of Eocene oceanic crustal rocks, probably emplaced in the same tectonic event as the Pacific Rim Terrane (Hyndman et al., 1990). To the west of these terranes lies the modern accretionary complex, which has formed since the Eocene by the scraping off of

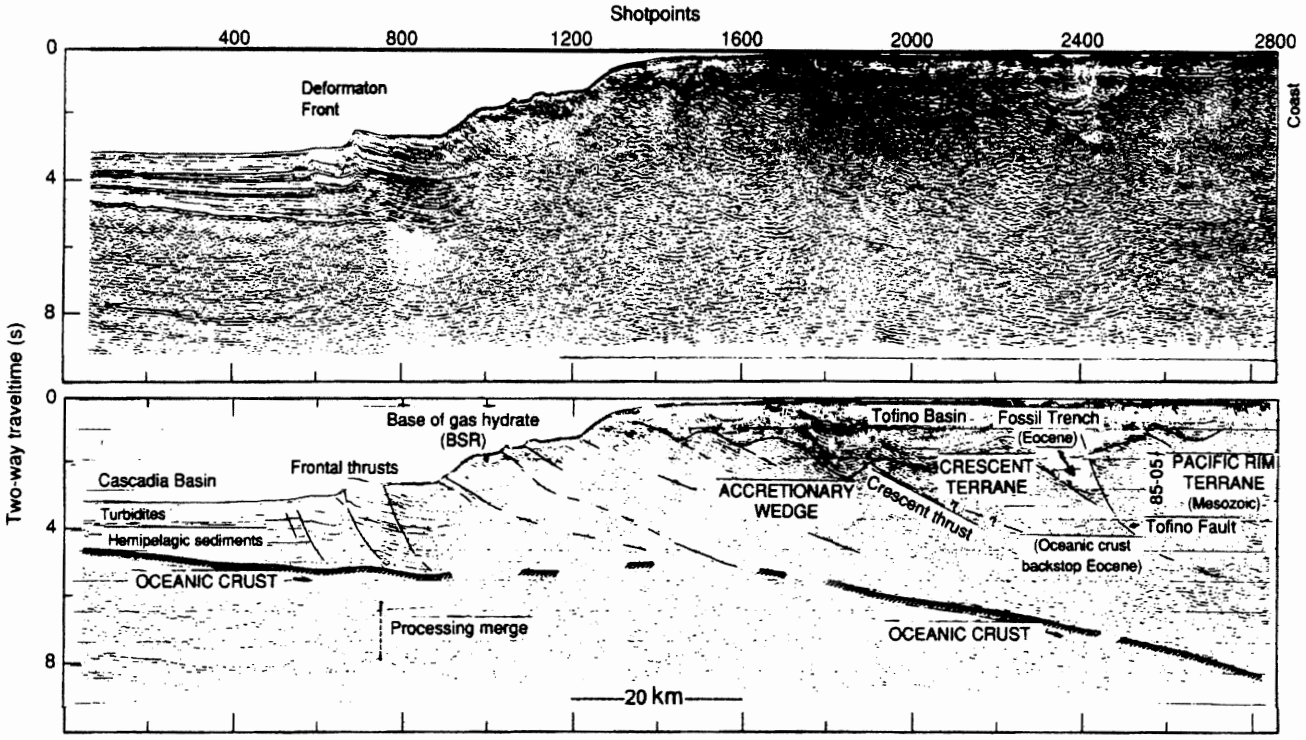

Figure 1.3. Multichannel seismic reflection line 85-01 section across the southern Vancouver Island Margin (LITHOPROBE). Vertical exaggeration is 3:1 for the upper MCS section and 1:1 for the lower section, showing the Cresent and Pacific Rim terranes at the landward end of the line and the deformation front of the accretionary prism towards the ocean (from Hyndman, 1995).

incoming sediments from the subducting Juan de Fuca Plate. The Tofino Basin (Fig 1.3) then covers the continental shelf sequence and contains mainly Eocene to Holocene marine clastic sediments (Yorath, 1987).

1.3.2. Accretionary Prism

The area of interest for the study of methane hydrates is located at the modern accretionary wedge, approximately 100 - 120 km offshore. Since the Eocene, the accretionary wedge off Vancouver Island has accumulated a 2- to 3-km thick sediment section from the subducting Juan de Fuca Plate (Hyndman, 1995). More than half of this section consists of Pleistocene turbidites, which overlie a thinner sequence of hemipelagites and fine-grained turbidites (von Huene and Kulm, 1973). The modern accretionary prism is characterized by deformation and east-dipping thrust faults which extend to the subducted oceanic crustal basement. This results in the formation of mounds and 'piggy-back basins', which are essentially a topographic low where incoming sediment from the continental shelf is deposited. In this section of the northern Cascadia Margin, in contrast to the central section off Oregon, most of the sedimentary section is being transferred to the North American Plate, and little sediment is subducted (Davis and Hyndman, 1989; Spence et al., 1991). This process is responsible for high pore pressures in the accretion zone and sediment underconsolidation, which leads to fluid expulsion (Hyndman, 1995).

1.3.3. Methane hydrate occurrence

The primary indicator of marine methane hydrate is a bottom simulating reflector (BSR) which parallels the seafloor in multichannel seismic sections (Fig. 1.4a.) (Shipley et al., 1979). The BSR is believed to mark the base of the stability field of methane

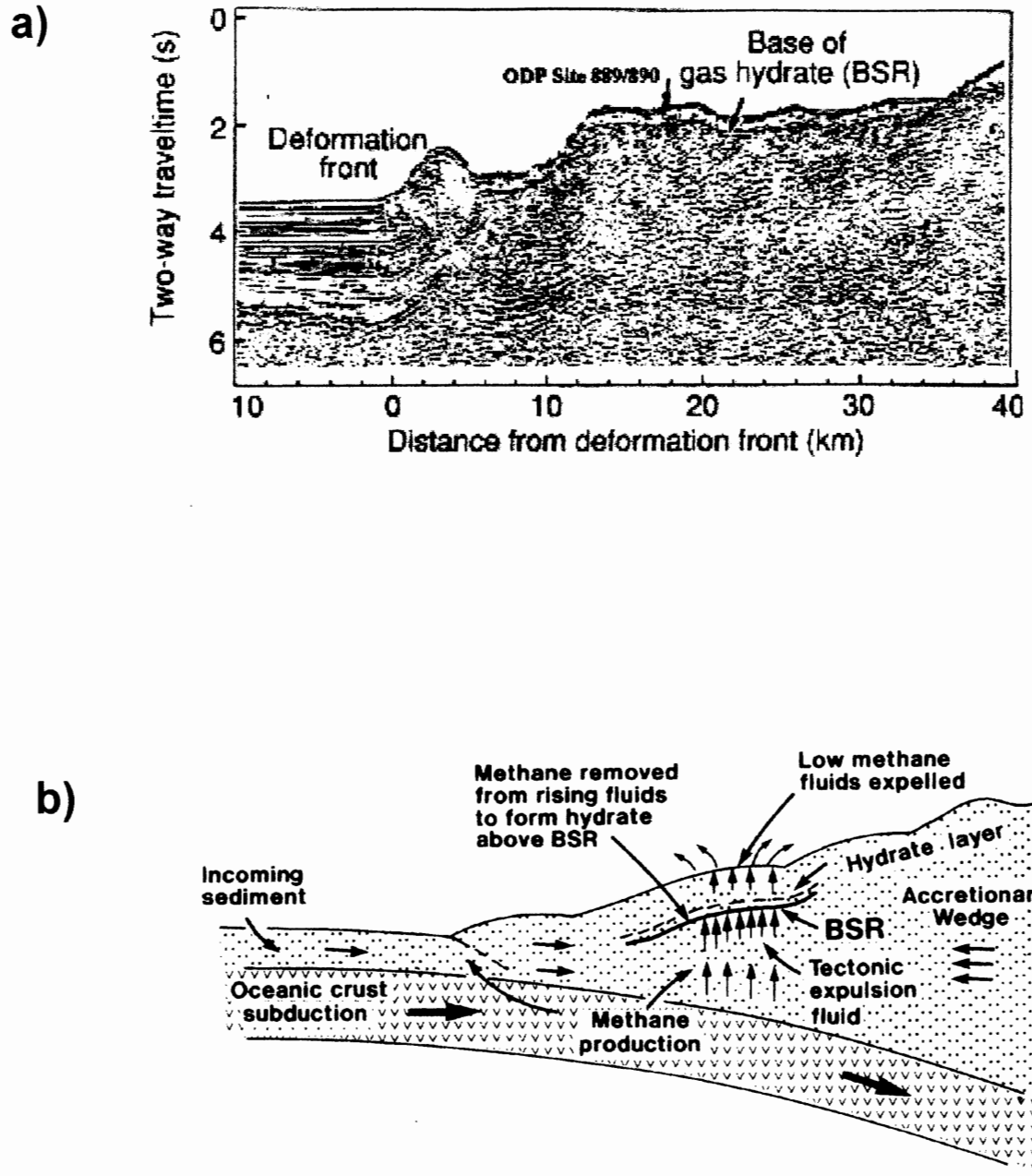

Figure 1.4 a) Seismic line 85-02 (LITHOPROBE) which shows BSR from base of gas hydrate layer (from Hyndman, 1995). b)Fluid expulsion model for methane hydrate formation near subduction zone (from Hyndman and Davis, 1992). As fluids are expelled from underlying compacted sediments, they pass into the hydrate stability field, and methane is removed from the fluids to form hydrate.

hydrates, and therefore the base of higher velocity sediments within the hydrate zone. The resulting high acoustic impedance contrast with the underlying sediments explains the BSR occurrence on reflection profiles. The methane hydrates (as indicated by BSRs) of the Cascadia Margin off Vancouver Island occur at approximately 200 – 250 metres below sea floor along the deformation front at the toe of the accretionary prism (approximately 120 km offshore) (Fig 1.4a.). The amount of methane hydrates in this location has been proposed by Hyndman and Davis (1992) to be the result of fluid expulsion from the compacted sediments beneath the hydrate layer (Fig 1.4b). As the fluid passes into the lower temperature regimes, it loses methane in the form of hydrates into the pores of the sediments.

1.4 Thesis Outline

Chapter 2 of this study will summarize the models of formation and genesis of methane hydrates in more detail. It will present various seismic studies which pertain to the methane hydrates and the BSR on the Cascadia Margin, as well as ODP drilling results. Chapter 3 will outline the data acquisition and logistics of the seismic survey which pertain to this study. Chapter 4 will outline the data characteristics and modelling procedures, followed by a detailed analysis and interpretation of the wide-angle seismic data. Chapter 5 will be a brief summary of the results and interpretations of this study.

CHAPTER 2 METHANE HYDRATES: FORMATION AND CHARACTERISTICS

2.1 Properties

2.1.1 Occurrence of methane hydrates

Marine gas hydrates consist of rigid water molecule cages stabilized by enclosed gas molecules, notably methane (Sloan, 1990). Figure 2.1a shows the phase diagram of pure methane hydrate with assumed thermal gradients in the subsurface regime of deep-sea sediments. The gas-hydrate phase boundary commonly occurs in marine sediments at depths of 100 – 300 m below the seafloor, where water depths exceed 300 m. This phase boundary parallels the seabed, often cutting across the stratigraphy, as it is temperature dependent and follows sub-seabed isotherms. The phase boundary is shifted by the present of trace gases and ions (eg. presence of NaCl and N_2 shift the phase boundary towards lower temperatures; CO_2, H_2S, and higher-molecular weight compounds shift the phase boundary towards higher temperatures.) (Kvenvolden, 1993).

Laboratory conditions of pressure/temperature stability zones of methane hydrates compared with observations of pressure and temperature conditions from DSDP/ODP borehole data are shown in Figure 2.1b. The stability field predicted which best fits the occurrence of methane hydrate is that estimated for artificial seawater from an equation of state (Engelzos and Bishnoi, 1988) (Fig. 2.1b). In the case of Cascadia Margin methane hydrates offshore Vancouver Island, pressures are approximately 17-18 MPa, and temperatures are approximately 16.8 °C (Hyndman et al., 1992), which are generally within the lower part of the pressure/temperature regime compared to other methane hydrate fields.

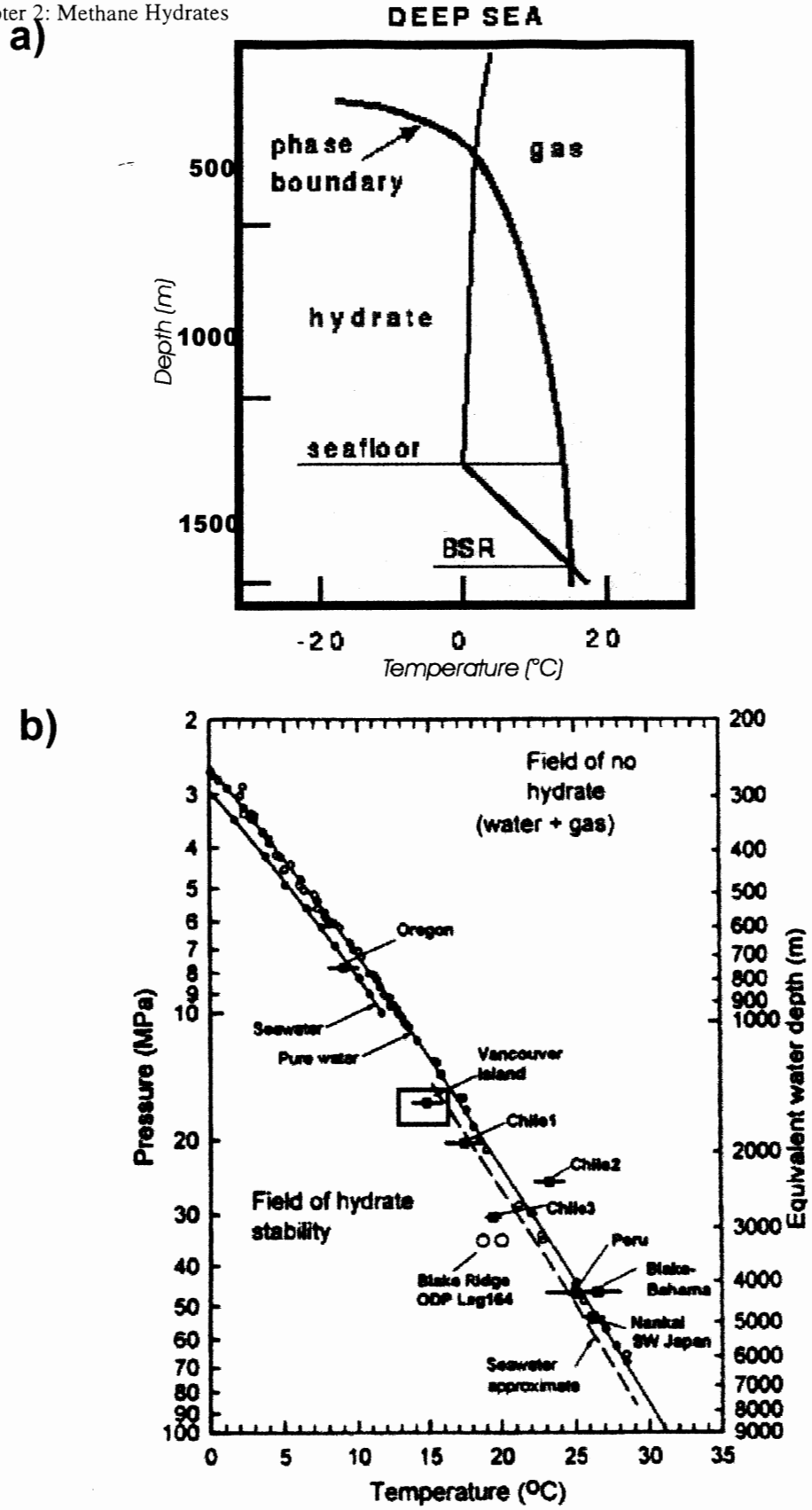

Figure 2.1 a) Simplified phase diagram of hydrates in pure methane/water system adjusted to typical conditions found in deep sea sediments (after Kvenvolden, 1993). Hydrate stability regimes below the sea floor are marked by the yellow zone. b) Compilation of hydrate stability zone pressure/temperature data from DSDP/ODP boreholes compared to laboratory conditions (P/T). Vancouver Island margin data is in the relatively lower P/T regimes (~16.8° C, 15 - 16 MPa) (outlined in red) (from Hyndman et al., 1992).

2.1.2 Physical properties of hydrates and hydrated sediments

P-wave velocities of marine hydrates were first calculated by Whalley (1980) to be ~3.8 km/s. Laboratory data and sonic logging through a massive gas hydrate layer yielded a P-wave velocity of ~3.6 km/s (von Huene et al., 1985). Sediments in which hydrates replace part of the pore water are consequently assumed to have higher seismic velocities than non-hydrated sediments (~1.7-1.9 km/s). The increase in P-wave velocities solely as a result of hydrates in pore spaces is difficult to estimate, as hydrates might not only replace pore water, but might also induce cementation between grains (Lee et al., 1994). While the replacement of pore water with hydrates is assumed to inhibit the processes of consolidation and mineral cementation, hydrates can act as cementation agents which increase the stiffness of the sediments (Kvenvolden, 1993), thus increasing the velocity.

The relation between velocity enhancement and hydrate concentration depends upon the degree to which the hydrate forms at grain boundary contacts or in the main pore spaces (Dvorkin et al., 1991). However, measurement of this is problematic and little data has been presented on grain-scale distribution. Another approach is to obtain a velocity for the combination of pure hydrate and sediment matrix (ie. no pore fluid) and the velocity of a water saturated sediment to determine the overall model velocity (Lee et al., 1993). The process is summarized by the following equation (Eqn. 2.1):

$$1/V_{hysed} = \phi/V_{hyd} + (1 - \phi) / V_{sed} \qquad (2.1)$$

where V_{hyd} is the velocity for pure hydrate (~3.730 km/s (Sloan, 1990)), V_{hyd} is the velocity for pure hydrate, ϕ is the porosity, and V_{sed} is the matrix velocity. Figure 2.2 shows a plot of velocity versus hydrate concentration in a sediment for V_{sed}=1600 m/s

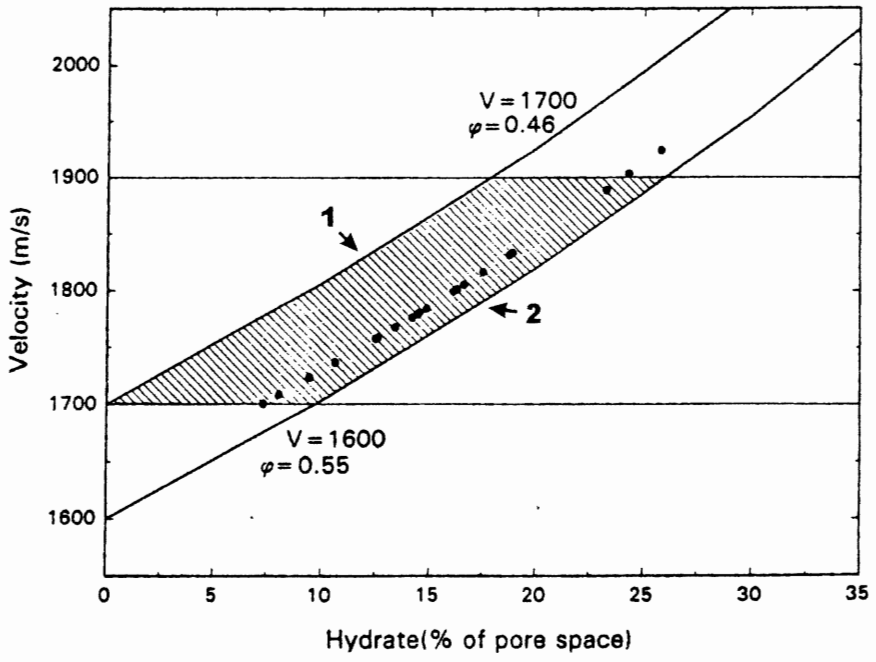

Figure 2.2. Sediment velocities enhanced by hydrate concentration from 2 sets of parameters: (1) hydrate- free velocity is 1700 m/s; fully hydrate-saturated velocity is 4120 m/s, for sediment porosity of 46%, and (2) hydrate- free velocity is 1600 m/s; fully hydrate-saturated velocity is 4040 m/s, for the sediment porosity of 55%. Measured velocities (solid dots) between 1700 and 1900 m/s suggest 10-25% of the sediment pore spaces are filled with hydrate (from Yuan et al., 1996).

and ϕ=0.55 and for V_{sed}=1700 m/s and ϕ=0.45 (Yuan et al., 1996). This kind of plot can be used to infer porosities based on seismic velocities and vice versa.

2.1.3 Formation mechanisms

Hydrates are generally considered to form entirely from bacterially generated methane as a result of low temperatures in the organic material in the sediments (biogenic methanogenesis) (Claypool and Kaplan, 1974). The first stage of biogenic methanogenesis results slightly after deposition as organic matter is oxidized by dissolving oxygen (Hesse, 1986). The second stage involves the reduction of organic matter by nitrates. Beneath this zone, sulfate reduction takes place until the next stage, in which methane is generated by carbonate reduction. The process of biogenic methane production is postulated only to take place in ventilated basins (Hesse, 1986). In some cases, the hydrate gas signatures may be consistent with a thermogenic origin (formation of methane through pressure-temperature condition changes) (Kvenolden et al., 1984), although this is not a likely mechanism for generation of as large amounts of methane and methane hydrates as biogenic methanogenesis.

Hydrates are known to occur in sediments as 1) finely disseminated, 2) small nodules having a diameter of less than 5 cm, 3) as layers separated from sediment layers, and 4) as massive hydrates (eg. DSDP Site 570: ~1.08 m long) (von Huene et al, 1985b). This is proposed to be the result of hydrate consolidation over time from a disseminated state (Brooks et al., 1985) based on the assumption of increasing thermogenic methane production with maturity of the hydrates.

It is believed that pore water has to be fully saturated with methane before natural hydrates can nucleate (Sloan, 1990; Paull et al., 1994; Brooks et al., 1994). Two main

models are proposed for the formation of methane hydrates. In the first model, formation can occur within the stability field itself with the right pressure-temperature conditions with perhaps some upward migration of free gas from below (Kvenvolden, 1993). However, with such high levels of hydrate inferred from geophysical investigations (ranging from 5% (Katzman et al., 1994) to 35% (Rowe and Gettrust, 1994)), Paull et al. (1994) suggest that the hydrate layers above BSRs are formed through an additional source of methane from upward-moving pore fluids as they pass into the stability field (Fig. 1.4b). Hydrates may then form either from methane bubbles driven by buoyancy or migrating fluids. The process of subduction zone sediment accretion and compaction results in strong upward fluid expulsion (Hyndman and Davis, 1992), which may account for increased hydrate occurrence in these zones. Diffuse fluid expulsion requires porous sand-dominated accretionary prisms (eg. Cascadia Basin turbidites and hemipelagic sediments).

2.2 Seismic characterization of methane hydrates: BSR

In situ information from deep sea drilling is limited; thus, much of the information on the formation of the hydrate zone has come from seismic reflection data. The detection of methane hydrates has been primarily through observation of a strong bottom-simulating reflector (BSR) (as discussed in Chapter 1). Seismic analyses include (1) determination of BSR reflection coefficients, (2) modelling of the vertical-incidence reflection waveforms, (3) multichannel velocity-depth analysis with wide-angle seismic data, (4) analysis and modelling of amplitude and waveform vs. offset (AVO), and (5) full waveform modelling.

Spence, Minshull, and Fink (1995) found that the BSR is not commonly observed in regions where significant thicknesses of slope basin sediments occur, but is most clearly seen where other sediment reflectors are weak or absent at the level of the BSR (Fig. 2.3). The BSR is postulated to still be present in the basin slopes though it is masked by stronger stratigraphic reflectors. The crucial unresolved question is how the strength and continuity of the BSR is linked to the amount and concentration of the methane hydrates. Similarly, does the absence of a strong BSR indicate an absence or reduced amount of methane hydrates above the BSR or changes in the amount of free gas below the BSR? Thus, recent studies (including this particulary study) are being undertaken using wide-angle and normal-incidence data to infer the P-wave velocity field of the sediment above the BSR in regions with strong and weak reflections, thus inferring an estimated hydrate content and concentration of the sediments in both areas.

The BSR is known to have a high negative impedance contrast (with reflection coefficients close to that of the seafloor, ranging from 20 – 30%) (Hyndman and Spence, 1992 b). There is some debate as to whether this high impedance contrast results mainly from a high- velocity hydrate zone above the BSR or to low velocity gas-saturated sediments below the BSR. Different studies have produced evidence for both sides of the argument. In the area of the Ocean Drilling Program (ODP) 889/890 sites (Leg 146) on the lower slope of the Cascadia margin off Vancouver Island, Hyndman and Spence (1992) concluded from high resolution velocity analysis of multi-channel seismic data that a high-velocity layer existed above the BSR, having a sharp base and a transitional top (Fig. 2.4a). No velocity or amplitude vs. offset effect of free gas below the BSR was detected. However, Singh and Minshull (1994) concluded that a low velocity gas layer

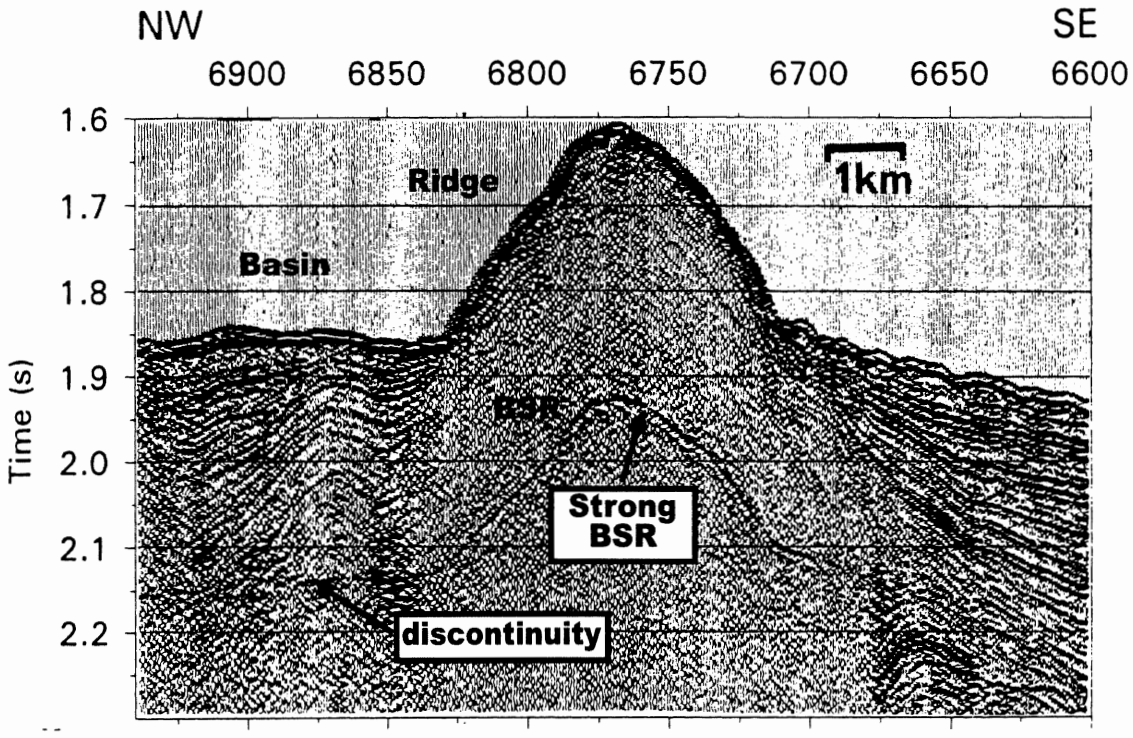

Figure 2.3. BSR discontinuity occurs along regions of slope basin sediments, while the BSR is relatively strong and continuous along ridge structures (after Spence, Minshull, and Fink (1995)).

a)

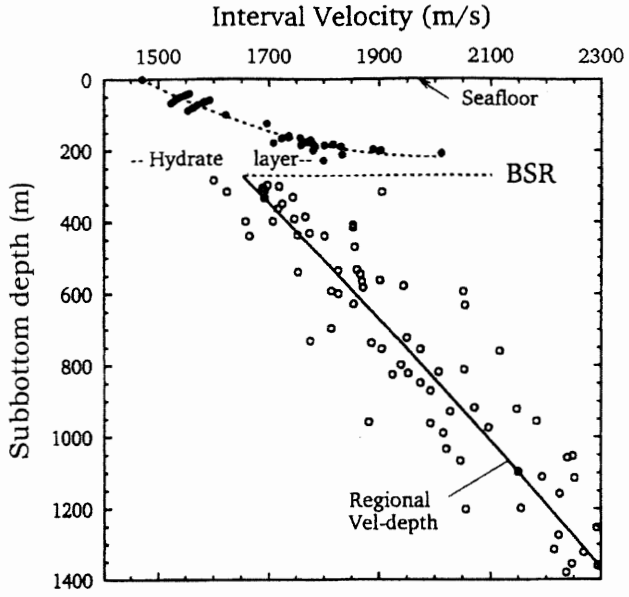

b)

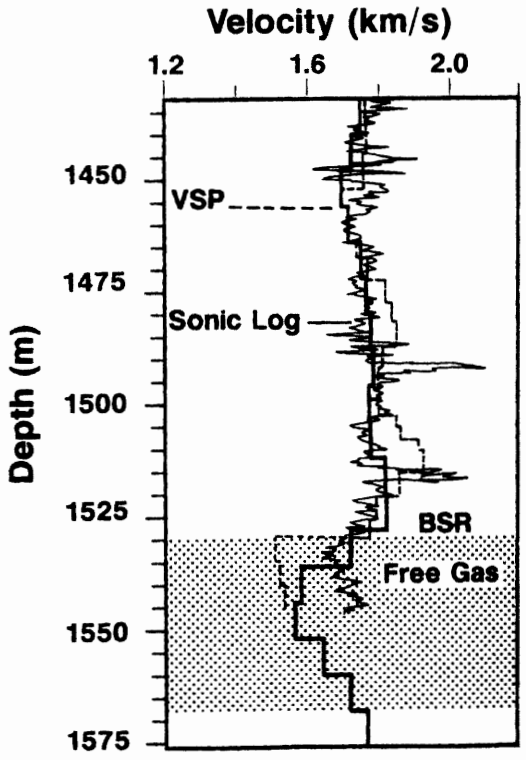

Figure 2.4 a) Interval velocity-depth data from detailed analysis of a short section which does not show a low velocity zone indicative of free gas beneath the BSR (from Hyndman and Spence, 1992). b) Velocity variations at ODP site 889 derived from a vertical seismic profile (VSP) (dash line) and sonic log (light line) (after MacKay et al., 1994). Singh and Minshull (1994) predict velocities from surface reflection data dark line which matches well with ODP results. The low-velocity zone is interpreted as partially saturated with methane gas (from Singh and Minshull, 1994).

was present based on full waveform inversion of the multichannel data of Hyndman and Spence (1992) (Fig. 2.4b). Yuan et al. (1996) concluded that the hydrate above the BSR accounts for ~2/3 of the impedance contrast required to produce the BSR reflection amplitudes, and that the remainder of the impedance contrast is associated with the free gas layer below the BSR, which is only resolved in the downhole VSP data (as opposed to MCS waveform inversion). Debate still exists as to the nature of the acoustic impedance contrast; namely, is the BSR a high velocity lid or is it mainly the result of a low velocity zone?

2.3 ODP drilling results

No pressurized-core barrel recovery of methane hydrates *in situ* was successful in the Cascadia Margin area, which would have lead to better analysis of hydrate properties (Westbrook et al., 1994). Methane hydrates in sediment cores of ODP drill sites are commonly indicated by indirect evidence, as the hydrate decomposes during core recovery due to change in pressure and temperature conditions. However, evidence such as gas-production induced voids, low temperatures as a result of endothermic dissociation of hydrates, and chemical markers (chlorinity and ^{13}C fractionation) can be used to infer the presence of hydrates. Geophysical logs can also clearly delineate methane hydrate zones, usually characterized by a decrease in density, an increase in P-wave velocity, and an increase in resistivity.

Controversy exists as to the amount of hydrate directly above the BSR and the amount of free gas present beneath this hydrate zone. Downhole logging and vertical seismic profile (VSP) data at ODP Site 889, Leg 146 indicated low velocities immediately below the BSR that implied the presence of free gas (MacKay et al., 1994) (Fig 2.5). MacKay

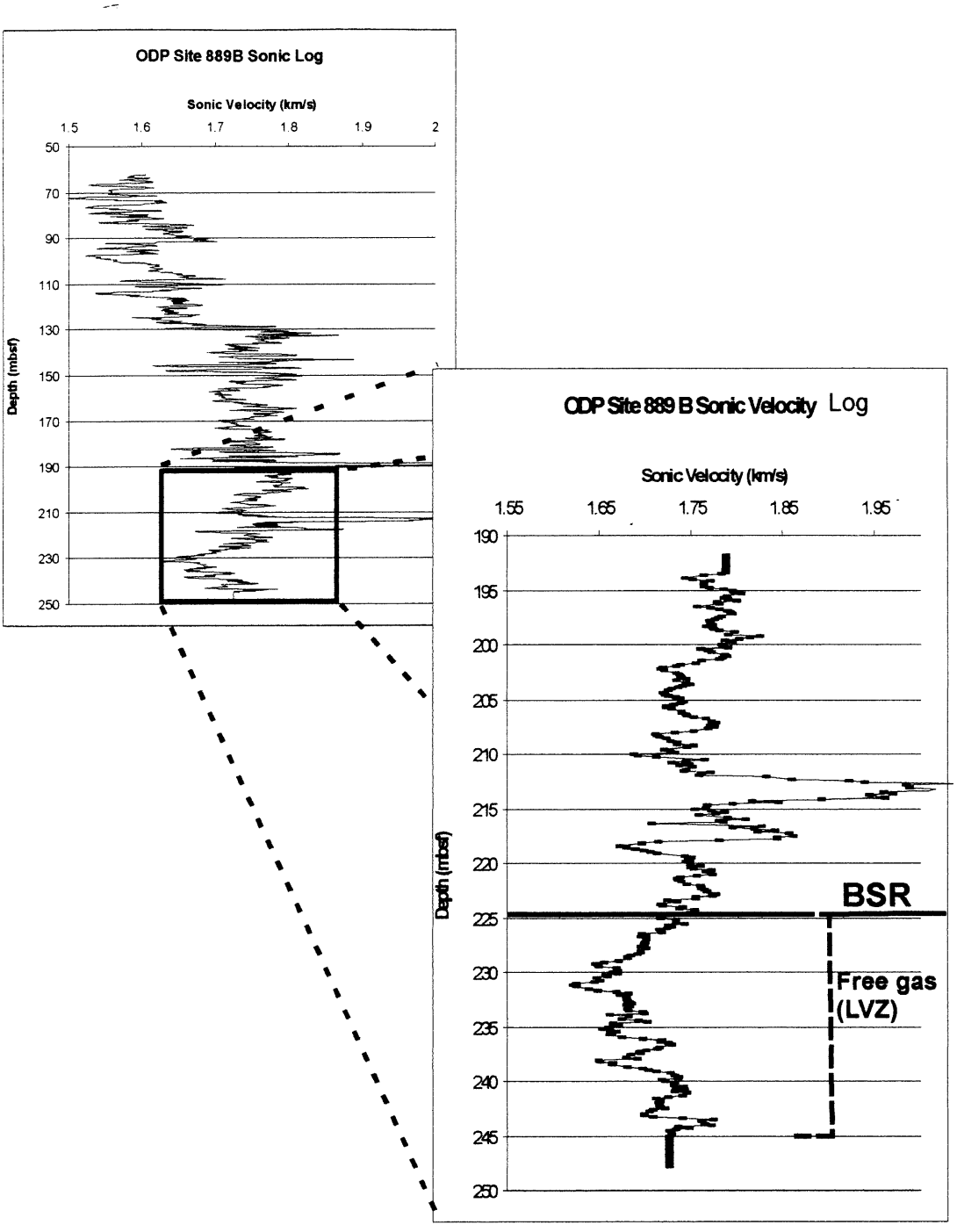

Figure 2.5. ODP sonic velocity log for site 889 (B) showing presence of low velocity gas zone. Depth is shown as metres below sea floor (mbsf) (from Leg 146 Cascadia Margin well- log data CD-ROM.)

et al. (1994) concluded that the velocity increase resulting from hydrate above the BSR on the Cascadia Margin was minimal, and that the hydrate mainly occurred in finely disseminated form. Westbrook et al. (1994) concluded the BSR resulted from the top of the thin low-velocity gas layer (~25 m) of no more than 5% free gas. In contrast, full waveform inversion studies on the Blake-Bahama Ridge have indicated a sharp velocity increase above the BSR ~ 15 m thick (1.8 - 2.3 km/s), indicating densely concentrated hydrates at the base of the stability zone (Korenaga et al., 1997). Furthermore, ODP drilling results from the Blake-Bahama Ridge (ODP Leg 164) indicate large amounts of free gas beneath the BSR (~ 200 m) (Holbrook et al., 1996), which are interpreted as being responsible for the sharp increase in the amounts of methane hydrate above the BSR. Based on the unresolved issues mentioned above, it would seem that there is some global variation in methane hydrate and free-gas concentrations in areas where BSRs occur.

CHAPTER 3 DATA ACQUISITION

3.1 Logistics of PGC- UVic Survey

The Pacific Geoscience Centre (PGC) and the School of Earth and Ocean Sciences, University of Victoria (UVic) conducted a multichannel seismic survey cruise on the central Vancouver Island margin (Fig 3.1) from 12 – 31 May 1997 aboard the research vessel C.S.S *John P. Tulley*. The objective of this expedition was to determine shallow seismic structure using a high resolution seismic survey and ocean bottom seismometers at sites where BSRs were previously known to occur.

The first phase of the cruise involved high resolution seismic profiling using the DTAGS (Deep Towed Acoustics-Geophysics System) of the U.S.Naval Research Laboratory. The deep towed source was towed at depths of approximately 300 m above the sea floor. Sound sources were triggered every 30 s while the ship proceeded at velocities of 2 to 3 knots. These data are recorded on 5 ocean bottom seismometers (OBS) deployed for the period when the DTAGS was operating. The second phase of the cruise involved the redeployment of 6 OBS for the collection of seismic data using surface airgun sources (40, 120, 300 cubic inch (cu. in.)). The air guns were towed at depths of 6 – 10 m, and were fired at intervals of 15 s at a ship speed of 5 to 6 knots. Dominant frequencies are approximately 150 Hz for the 40 cu. in. air gun, 75 Hz for the 120 cu. in. air gun, and 30 Hz for the 300 cu. in. air gun. This second phase of the seismic survey using airgun sources produced higher resolution wide-angle seismic reflection data, therefore, this particular analysis uses seismic lines from this phase.

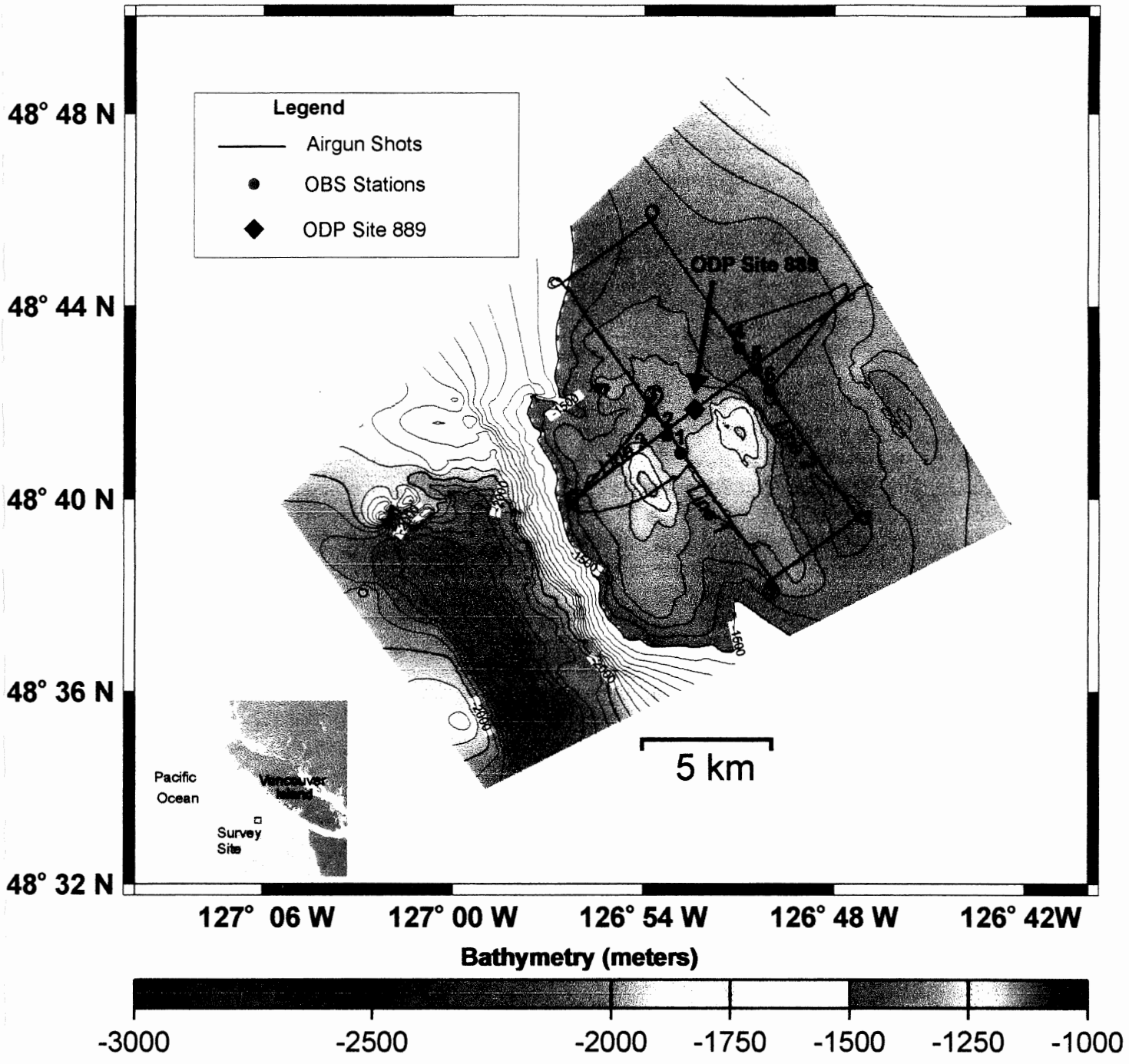

Figure 3.1 Bathymetric map of survey site area for Pacific Geoscience Centre cruise (1997) displaying OBS positions, (OBS 1 - 6), wide angle seismic lines (Lines 1- 3), and ODP Site 889. OBS 1 is located on higher topography than OBS 6 (approximately 5 km apart).

3.2 Survey Site

The seismic survey lines which pertain to this analysis consisted of: 1) two lines (approximately 12 km long) each parallel to the 1300 m depth contour with 3 OBS stations along each line (Line 1: OBS 1, 2, 3, and Line 2: OBS 4, 5, 6; and 2) one line perpendicular to depth contours approximately 5 km long which crosses these two parallel lines towards their respective midpoints (Line 3: OBS 2 and 5) approximately 5 km in length (Fig. 3.1). The experiments were carried out in water depths between 400 and 2200 m along the continental slope.

The seismic data recorded which pertain to the velocity-modeling of wide-angle reflections and refractions in this study were data collected from OBS 1, Line 1. Figure 3.2 shows the relative position of OBS 1 and 6 (parallel to Line 3 in cross section) with respect to ODP Site 889 on the single channel seismic reflection profile taken during the cruise. OBS 1 is positioned over a ridge structure on the deformation front close to ODP Site 889 (within approximately 1.5 km away) over an area where a strong BSR occurs, while OBS 6 is stationed over a basin structure approximately 5 km northeast of OBS 1. The position of these OBSs is important in understanding the distribution of methane hydrates along areas where there is a strong BSR (ridge structures) and where the BSR is discontinuous (basin structure) with many stratigraphic markers.

3.3 Dalhousie Digital Ocean Bottom Seismometers (OBS)

The Dalhousie ocean bottom seismometer is a free-fall self contained seismograph which records 4-channel data: an externally mounted hydrophone and 3 internally mounted orthogonal component geophones (Fig. 3.3a). The specifications of the instrument are given in Table 1. The external packaging follows the design of previous OBS developed by the Bedford Institute of Oceanography (Atlantic Geoscience Centre, Geological Survey of Canada) (Fig. 3.4b).

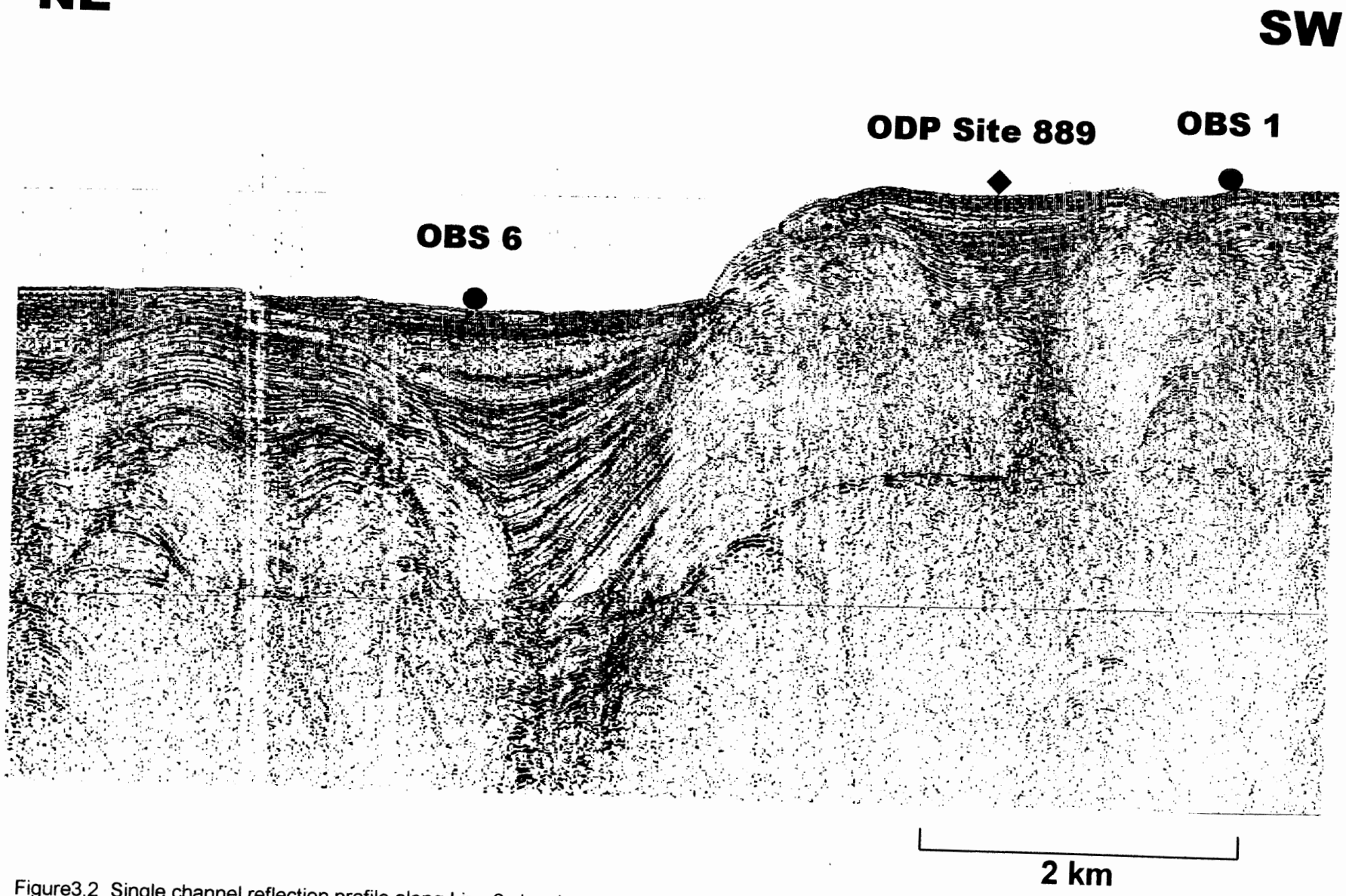

Figure3.2 Single channel reflection profile along Line 3 showing relative positions of OBS 1, OBS 6, and ODP Site 889. OBS 1 is located along a ridge structure; OBS 6 is located in the 'piggy-back' basin.

a)

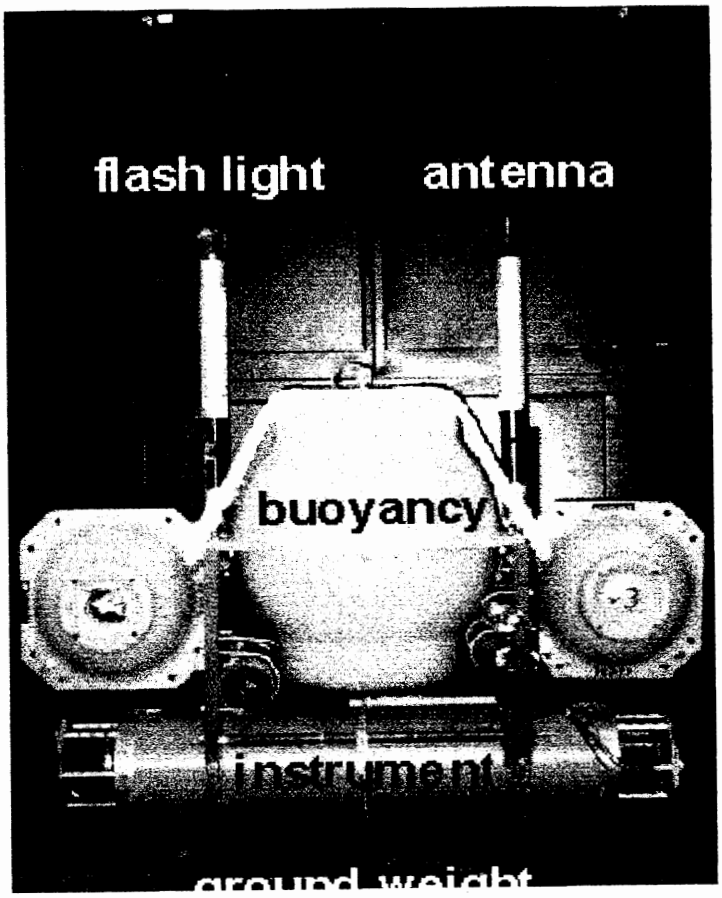

b)

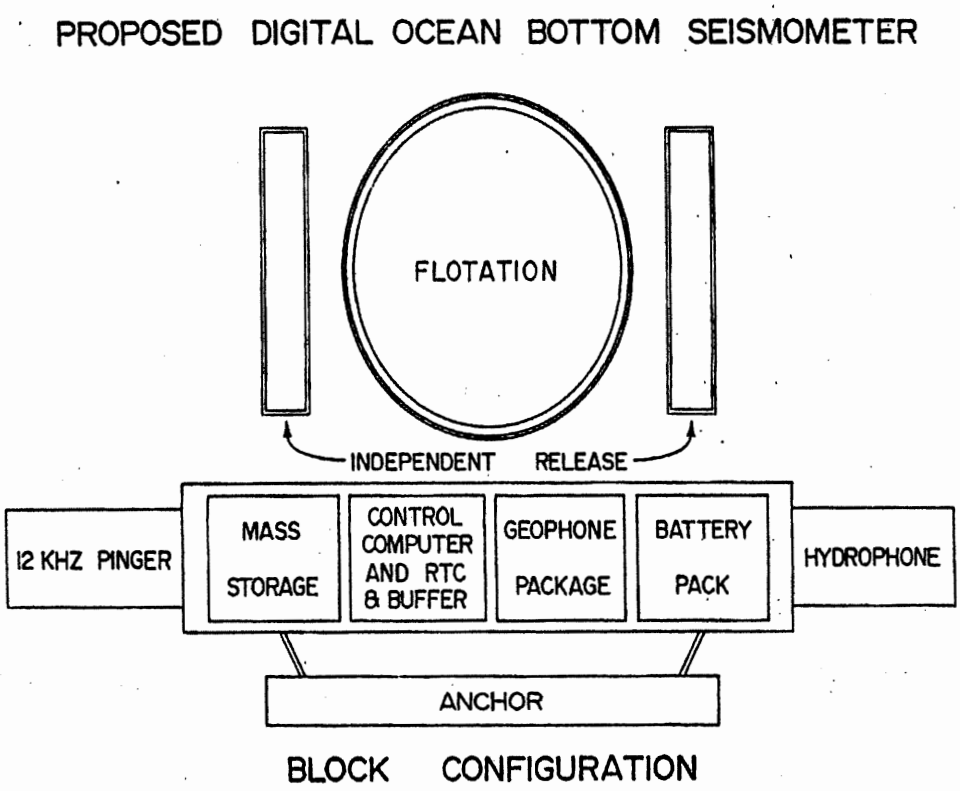

Figure 3.3 a)Dalhousie ocean bottom seismometer (OBS) external package photograph. b) Schematic of OBS displaying externally mounted hydrophone, internal geophone package, acoustic command and pinger, digital acquisition and data logger, and clock

Table 1 Dalhousie OBS Specifications

Item	Specification	
Housing/Platform	Uses existing design of BIO-OBS (6 km max water depth) weight in air: instrument (82 kg); anchor (55 kg) size (1.1 m high; 1.2 m long; 0.6 m wide)	
Release	12.5 kHz Acoustic command + timed backup	
Duration of recording	4.6 days @ 5.7 msec sampling of 4 chan (16 bit) 1.1 days @ 0.8 msec sampling of 4 chan (12 bit)	
Sampling rates / dynamic range	23/11.5/5.7/2.9/1.4 msec @ 16 bit (AD7716 Sigma-Delta ADC) 1.6/0.8/0.4/0.2 msec @ 12 bit (Tattletale 7 ADC)	
Anti-alias filter	switched-capacitor, software selectable with corner freqs of 12.5, 25, 50, 100, 200, 500, 1000 Hz	
Gain	Fixed settings hardware selectable geophones (69-93 dB); hydrophone (46-70 dB)	
Max electrical noise	< 125 nVrms on geophone input < 1uVrms on hydrophone input	
Clock	Austron 1115 OCXO 5 MHz(drift<1 msec/day)	
Data storage	2 Mb RAM stored as separate files on 540 Mb Connor HD w/ OTAK adaptor to TT7	
Sensors	3-component geophone package (oil filled): 4.5 Hz (Mark L-15B; 380 Ohm coil w/ 0.7 damping) 100Hz (Oyo GS-100; 975 Ohm coil w/ 0.7 damping) hydrophone (OAS E-2SD)	
External connectors	4-pin (RS-232 comm + time pulse) 3x1-pin (hydrophone+release)	
Batteries: data logger	4 C-cell lithium (clock) 12 D-cell NiCad (disk drive) 10+8, D-cell alkaline (analog+digital)	est. lifetime >10 days
acoustic release	2, 9-volt alkaline (electronics) 4+4, 9-volt alkaline (pinger+release)	
Data transfer rates to PC	TT7 parallel interface to AT-DIO-24 (100 kbyte/s)	
Recovery Aids	Strobe + Radio beacon (Novatech ST400A, RF700A-1) 12.5 kHz pinger (ITC 3013 transducer)	

Internal components of the seismometer consist of 4 modules: the 12.5 kHz acoustic command and pinger; the digital acquisition and data logger; the 3 – component geophone; and clock and battery packs. Digital data acquisition is performed on a Tattletale 7 (TT7) data logger with 540 Mb hard drive. The additional electronic components include an analog waveform acquisition unit, digital interface, and clock and power supply conditioning. The waveform acquisition board receives input analog from the geophone and hydrophone signals and applies gain and anti-alias filters. It then passes the analog output to the TT7 for high speed 12-bit or 16-bit ADC (analog to digital conversion). The digital interface board takes this converted data from 3 waveform acquisition boards (3 component geophones). It can then condition the clock signal for selectable digitization rates, as well as buffering the external trigger to set the real-time clock.

Seismic data are stored first in 2 Mb RAM, which includes a 512-byte header. When the RAM is filled, the contents are then moved onto the hard disk, taking approximately 30 seconds, during which data acquisition is interrupted (which is evident as blank spaces in place of shot traces in predictable time intervals). This process continues until the acoustic release transmits a release code, at which point all data acquisition terminates, and the final data are written to hard disk. Once the OBS is recovered, the data are written to an external disk, and archived to Exabyte tape.

3.4 Wide-angle Data Characteristics

Seismic processing involves using the shot table data file (logged by a remote PC) and merging these files with the OBS digital files to form a data file of shot records which follows industry standard SEGY format (Society of Exploration Geophysics). The precise depth and location of the shot source needs to be correlated with navigational data in order to determine the precise location of the OBS stations. This can be done by first correlating ship navigational data

with shot tables, then processing the data with these shot tables to give travel time vs. offset plots based on a known range of shot traces. Subsequently, updated SEGY files can be made with the correct ranges for the respective OBS. This data can then be modeled using forward modelling techniques for wide-angle relections and refractions to obtain a detailed velocity structure (as described in the following chapter).

Figure 3.4 shows an illustration of the techniques used to collect wide-angle seismic data. As opposed to vertical incidence reflection profiling, wide-angle seismic surveys are conducted in order to analyze the turning (or bending rays) within the sedimentary layers. When velocity gradients in the marine sediments are relatively high, rays bend through the sedimentary layers at relatively low offsets. At higher offsets, rays which pass through these high gradient layers no longer reach the surface (receivers). At low velocity gradients, rays bend relatively slowly. Thus, rays arrive at the surface (receivers) at relatively large offsets.

An example of a wide-angle reflection profile using OBS 1, Line 1 data for the 40 cu. in. airgun is displayed in Figure 3.5. This figure plots arrival times (with no reduction applied) against offset for negative and positive offsets. The reflection phases have particular velocities, which can be easier modeled by using plots such as reduction velocity and normal moveout correction (which is discussed in the following chapter).

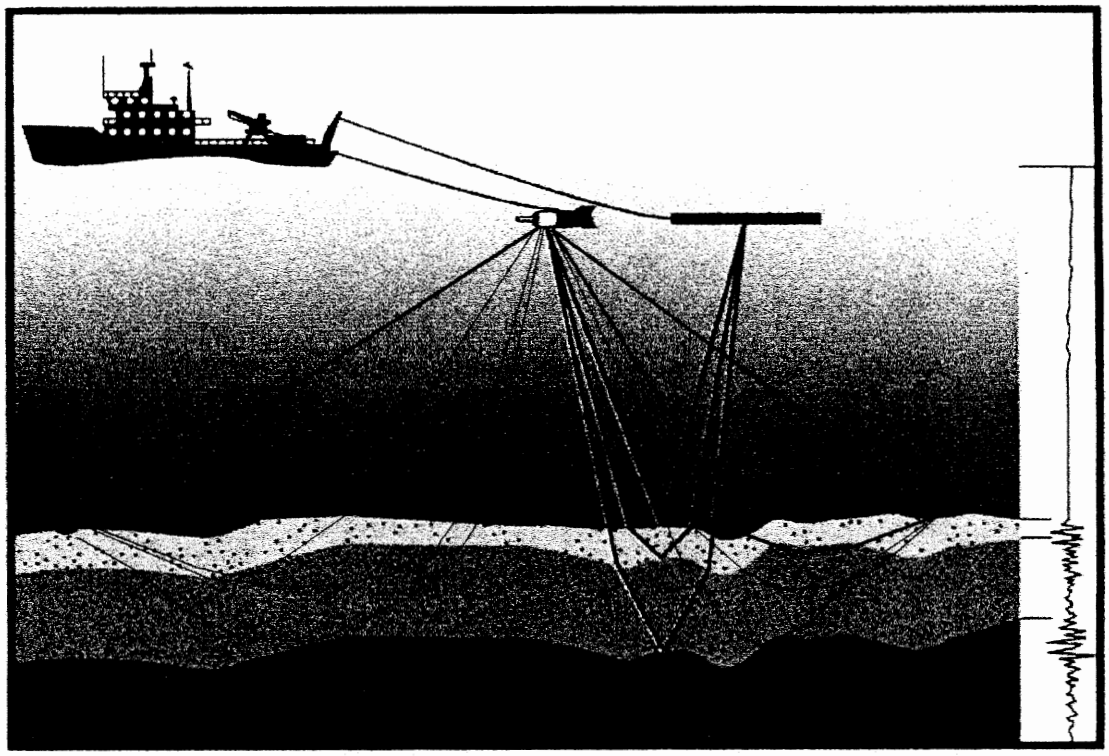

Figure 3.4 Cartoon illustration of vertical incidence seismic geometry with receivers being towed and wide angle seismic geometry with ocean bottom seismometers. The wide angle data geometry illustrates raypath bending as a result of velocity gradients in the sediment below the seafloor.

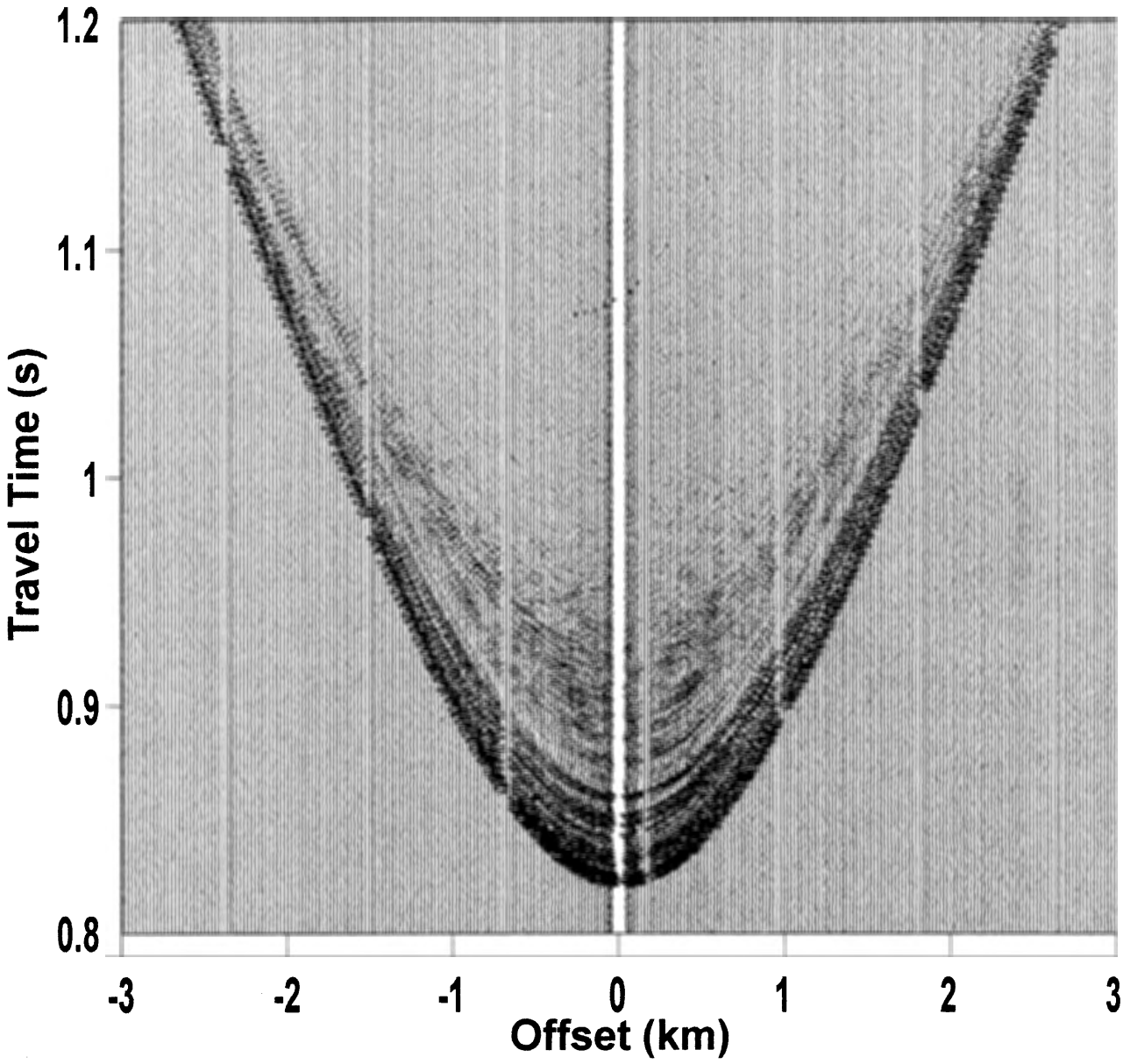

Figure 3.5 Travel time vs offset plot for OBS 1, Line 1 using 40 cu. in. airgun, showing direct arrivals and subsequent reflection arrivals.

CHAPTER 4 DATA ANALYSIS AND INTERPRETATION

4.1 Data Characteristics (OBS 1, Line 1)

Travel time vs. offset data are adjusted to a reduction velocity (V_r) of 2 km/s (plotted as (time - offset / V_r) vs. offset). Reduced travel time plots are a standard way of looking at wide-angle seismic data in order to see the curve of the reflectors and better analyze the turning ray arrivals with offset. The reduced travel time plots from OBS 1, Line 1 can be seen in Figure 4.1. The airgun sources used for modelling are the 40 cu. in. airgun and 300 cu. in airgun source. Positive offsets (towards NW) are plotted for the 40 cu. in. airgun (Fig. 4.1a) and for the 300 cu. in. air gun (Fig. 4.1b). Refraction arrivals are apparent as primary arrivals from the 300 cu. in. airgun source at approximately 4 to 5 km offset (Fig. 4.1b). No refraction arrivals are apparent as primary arrivals for the 40 cu. in. airgun source, most likely as a result of attenuation of higher frequency energy sources.

The bottom simulating reflector (BSR) is clearly visible from both airgun sources for OBS 1, Line 1 (Fig. 4.2). Nevertheless, the positive offsets along Line 1 for the 40 cu. in. airgun source (toward NW) display discontinuity in the BSR, and the BSR is generally more continuous with negative offsets (towards SE). Positive offsets display a relatively strong BSR with the 300 cu. in. airgun source along Line 1 (Fig. 4.2b). This is consistent with the higher amplitude of reflectors above the BSR, which are visible with the 300 cu. in. airgun data. This is the result of the relatively larger energy source, which also creates a larger bubble pulse. The bubble pulse (created by the expanding and contracting of the air released from the airgun) can also be seen with the 300 cu. in. airgun source, which is not visible with the 40 cu. in. source (Fig 4.2).

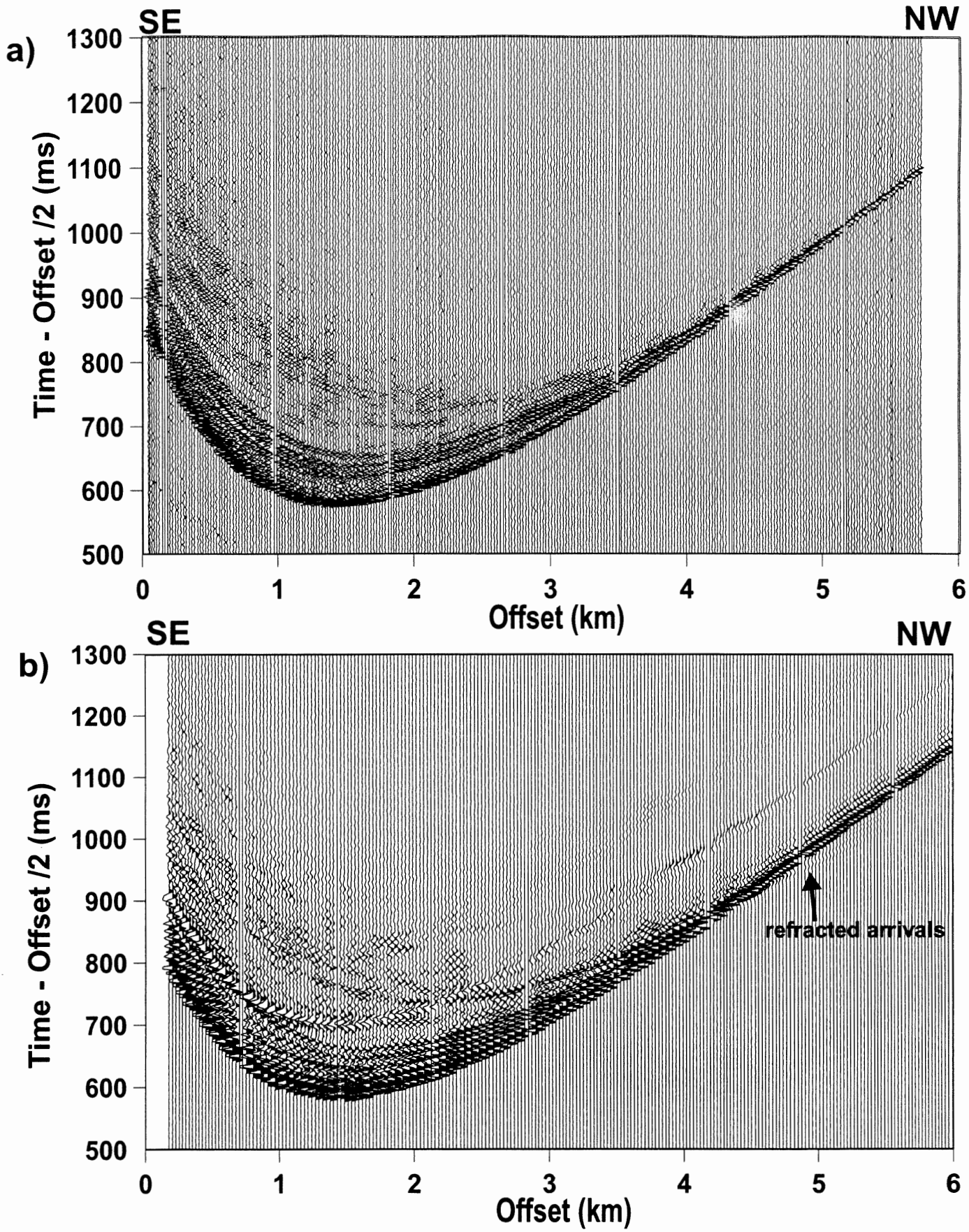

Figure 4.1 Reduced travel time vs. offset plot for OBS 1, Line 1 for a) 40 cu. in airgun source data, and b) 300 cu. in. airgun data for positive offsets. Refracted arrivals are visible with the 300 cu. in. airgun data (beginning at offsets ~ 4 km).

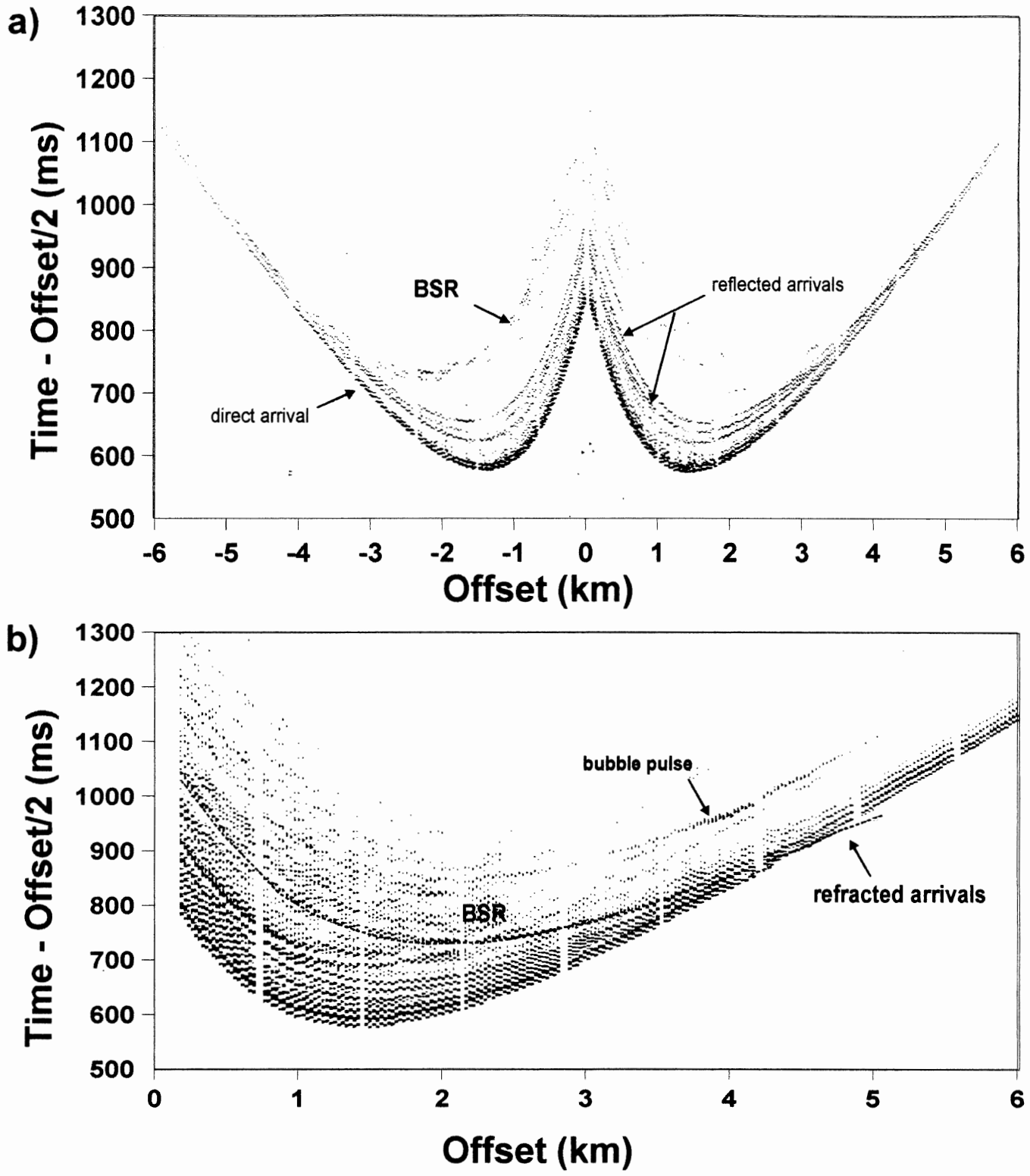

Figure 4.2 a) OBS 1 wide- angle reflection data for 40 cu. in. airgun source for Line 1. BSR is fairly continous along negative offsets (shots to SE). b) OBS 1 wide-angle reflection data for 300 cu. in. airgun for Line 1 (positive offsets only). The lower requency source creates a stronger bubble pulse. Refracted arrivals become primary arrivals at approximately 4.1 km offset (outlined in purple), with phase velocities of approximately 1.7-1.65 km/s. BSR arrivals are seen outlined in red.

4.2 Procedure

For modelling purposes, the OBS 1 data was displayed by using a normal moveout conversion for the water layer (ie. Layer 1). The water layer is known to have an average velocity of 1.481 km/s from bathythermographic data of the survey site (Fig 4.3). Converting travel times (t_r) to normal moveout corrected travel times (t_c) uses the equation:

$$t_c = t_r - t_o = (t_o^2 + x^2/v_w^2)^{1/2} - t_o = (h^2/ v_w^2 + x^2/v_w^2)^{1/2} - h/v_w \qquad (4.1)$$

where h is the depth to the bottom of the water layer, v_w is the velocity of the water layer, and x is the offset. Given t_o and v_w, the normal moveout corrected travel time can be calculated. A velocity of 1.481 is used for the water layer, and the depth to sea floor is input as 1.292 km (based on bathythermograph plots and reflection profile data (Fig. 4.3)). Normal moveout corrected data for OBS 1, Line 1 for the 40 cu. in. airgun data is shown in Figure 4.4. This correction is effective at separating the wide-angle reflection/ refraction phases by increased amounts at vertical incidence.

One-dimensional velocity-depth modelling of OBS 1, Line 1 data involved three distinct stages. The primary stages of modelling of the OBS 1 data was performed by entering distance-time coordinates for the reflection curves from the various interfaces into a computer program (PENTEX), which then computes the optimum velocity above the interface as well as the depth of the interface by minimizing a least-squares fit using the Dix equation (Eqn. 4.2).

$$V_{int} = [(V_{rms\ n}^2\ t_n - (V_{rms\ n-1})^2\ t_{n-1}) / (t_n - t_{n-1})]^{1/2} \qquad (4.2)$$

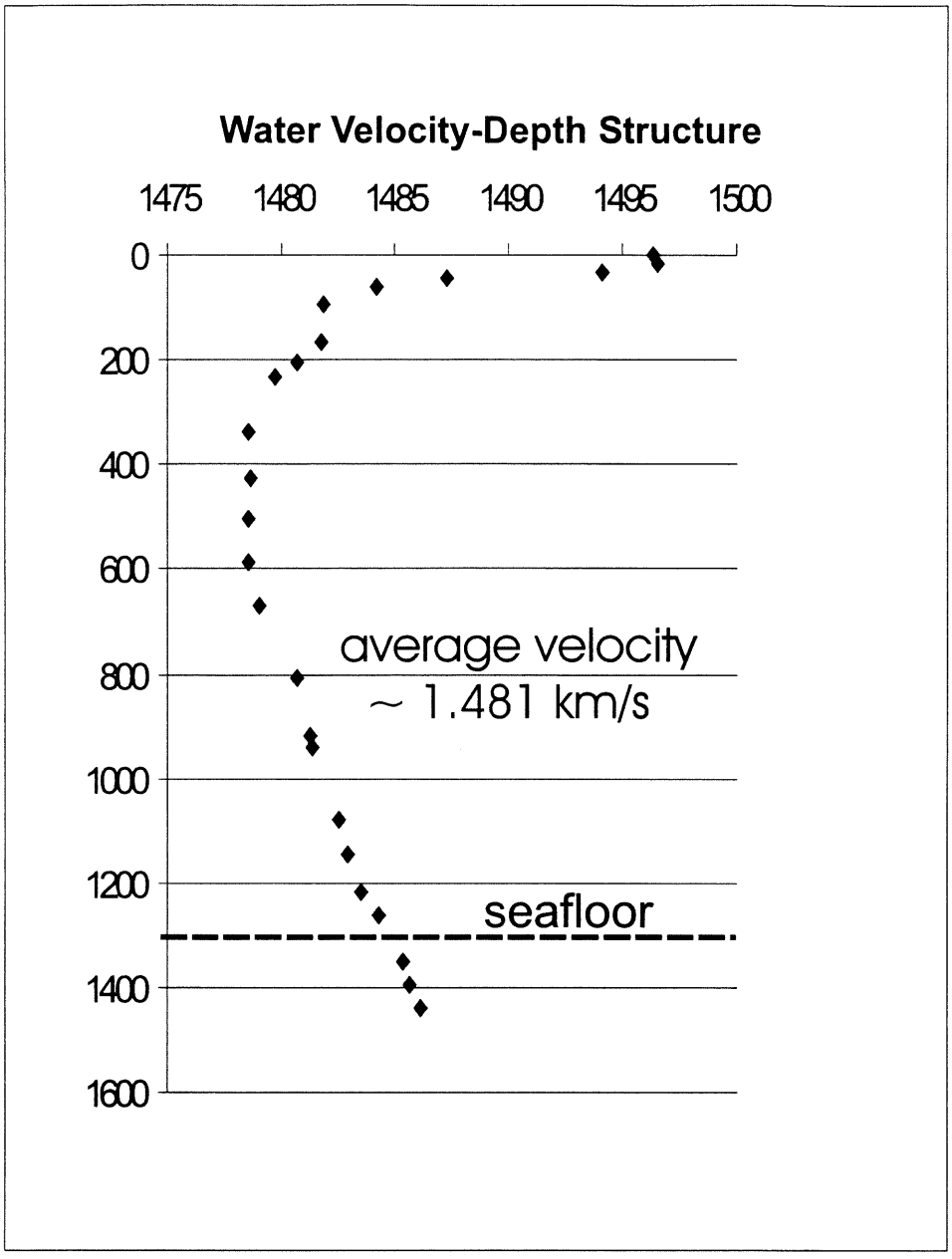

Figure 4.3 Water velocity structure for location of OBS 1 from bathythermograph plots of PGC cruise. Average (mean) velocity is calculated at 1.481 m/s. Seafloor depth is shown at approximately 1292 m (calculated from normal incidence travel times of seismic survey).

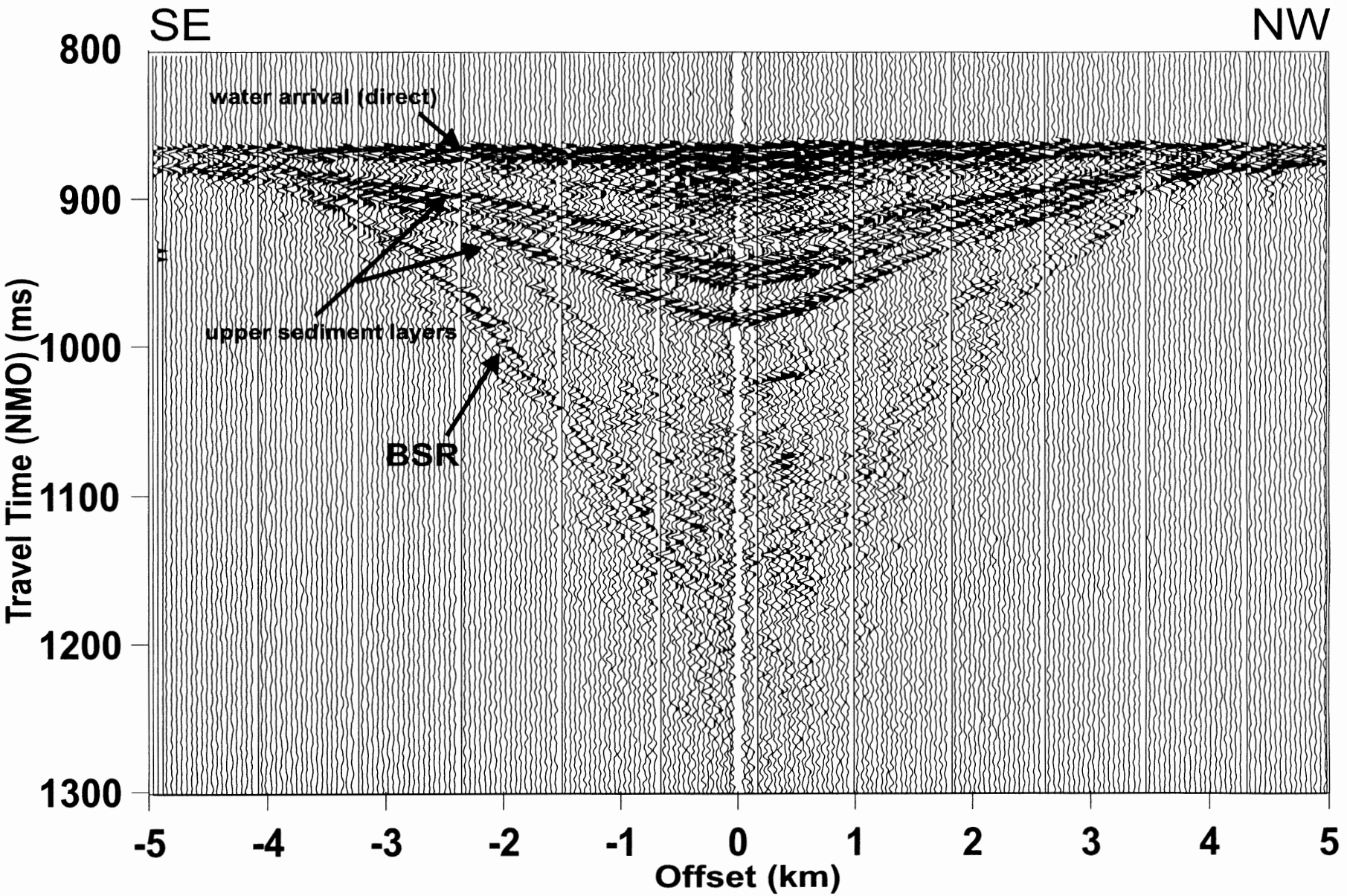

Figure 4.4 Normal moveout corrected travel time vs. offset wide angle reflection data using 40 cu.in. airgun (OBS 1, Line 1). The normal moveout correction better differentiates the reflected phases, making it more useful for modeling. The BSR appears strongly with negative offsets (SE), but is less continuous towards positive offsets (NW).

where V_{int} is the interval velocity, $V_{rms\ n}$ is the root means square velocity of a given layer, and $V_{rms\ n-1}$ is the root mean square velocity of the layer beneath that layer, t_n is the interval travel time of the given layer, and t_{n-1} is the total travel time above that layer. Velocities do not vary as gradients within the layers, but are output as one average velocity based on the travel time curves.

The following two stages of modelling used the ray tracing programs of Zelt and Smith (1992). This method allows the forward modelling of velocity gradient with depth, as the travel times from bending ray paths can be calculated. Travel times are calculated by numerical integration along ray paths in a two-dimensional media using the trapezoidal rule (Runge-Kutta method). A plot of the model and all rays traced may be produced along with a plot of reduced travel time vs. offset for the observed and calculated data. This ray tracing is applicable both to the fitting of travel times to both reflection and refraction data. A layer-stripping approach is used, where the model parameters are determined first for shallow depths, then fixed for calculation of deeper layer parameters. This method (known as forward modelling) is used for the second stage of modelling using the 40 cu. in. airgun source data for OBS 1, Line 1 to model the velocity-depth structures based on the reflected phases. The third stage also uses this method to model reflected and refracted phases visible from the 300 cu. in. airgun source, in order to better constrain the models using the 40 cu. in. airgun. The constraining of the velocity gradient is achieved by fitting the slopes of the refracted phase arrivals, as well as the cutoff points where the phase arrivals terminate (as discussed in Chapter 3).

4.3 Velocity Modelling Results

4.3.1 Preliminary Modelling: Model 1 (40 cu. in airgun source)

A five layer structure is modelled using the PENTEX program, not including the water layer. Only negative offsets (toward SE) reflection arrivals were modelled using this method. Velocities obtained from this model vary somewhat from the ODP Site 889B sonic log data (Fig. 4.5), although the trend of the model closely follows the sonic log data. The BSR fitted travel time curve has a slightly lower vertical incidence travel time than the data points, although the trend is consistent with greater offsets. This model predicts a depth of 239 metres below the sea floor (mbsf) for the BSR, and a velocity of 1.79 km/s in the layer above the BSR (118 - 239 mbsf). This model can then act as a satisfactory starting point for the subsequent ray tracing modelling methods.

4.3.2 Ray Trace Modelling: Model 2 (40 cu. in. airgun source)

After the preliminary modelling, travel time fitting from ray tracing (using Zelt's method) is overlain on the actual data rather than digitized arrival times. The water layer is adjusted to an average velocity of 1.482 km/s and a depth of 1.275 km. These modifications are made arbitrarily in order to better fit the calculated travel times with the first arrival, and are not crucial to the modelling of subsequent layers below the sea floor. The layer underneath the BSR is arbitrarily assumed to be 20 m thick with a velocity of 1.65 km/s based on ODP drilling results in order to produce an impedance contrast at the BSR, and does not affect the velocity gradient above the BSR.

Modelling of the normal moveout corrected data of OBS 1, Line1 using the 40 cu. in. airgun source produces the 2-D velocity model (which assumes lateral homogeneity) shown in Figure 4.6 (Model 2). Six layers are predicted to exist above the BSR, not including the water

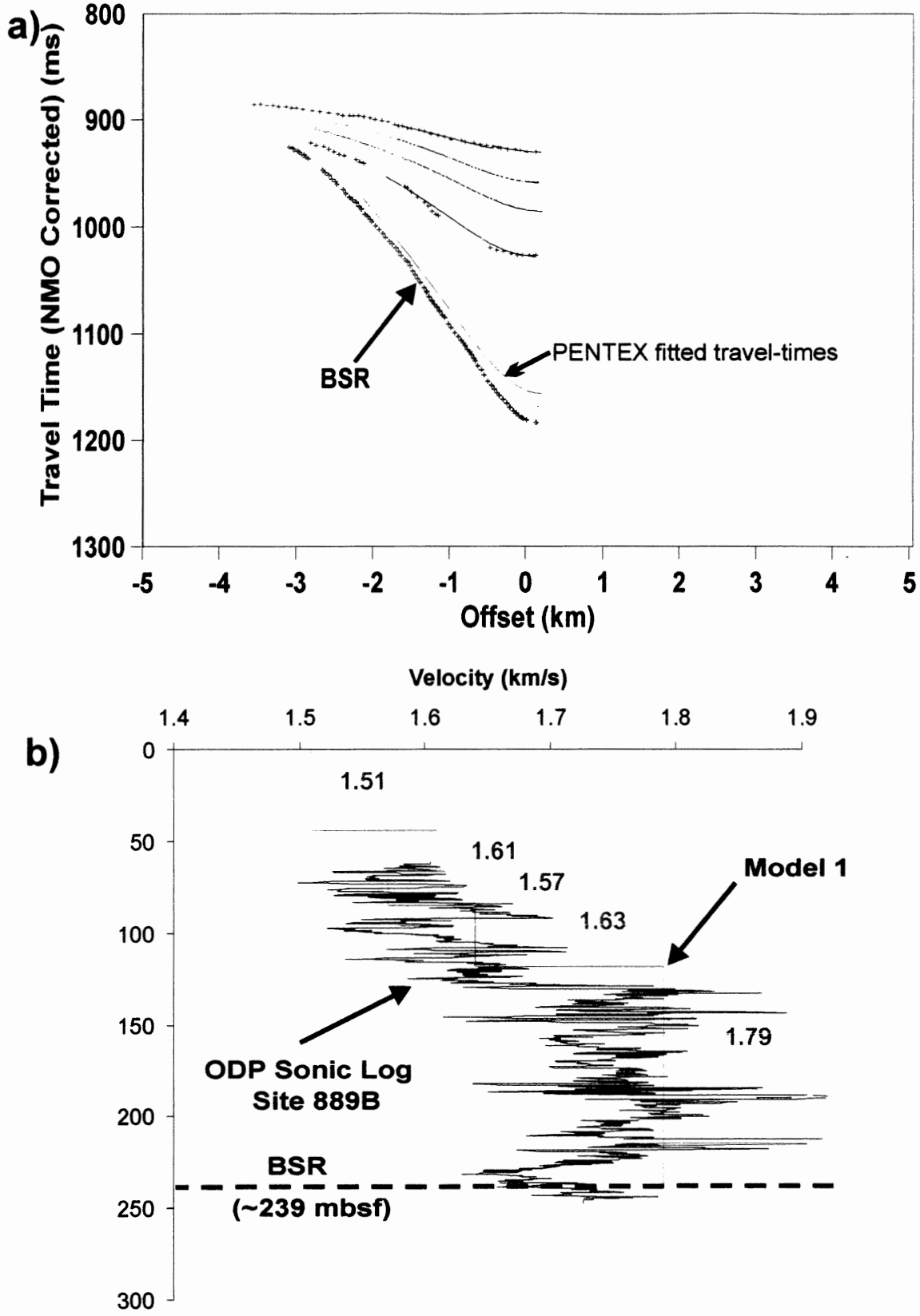

Figure 4.5 a) Digitized travel times and PENTEX results for 40 cu. in. airgun data (OBS 1, Line 1). BSR digitized travel times and PENTEX fitted travel times for BSR are outlined in red.
b) Preliminary velocity-depth model (Model 1 - outlined in pink) using PENTEX program displayed over ODP Site 889B sonic log velocities. This model assumes no velocity gradient within the layer boundaries. The layer above the BSR (methane hydrate zone) has a velocity of approximately 1.79 km/s. The BSR depth is estimated at 239 mbsf.

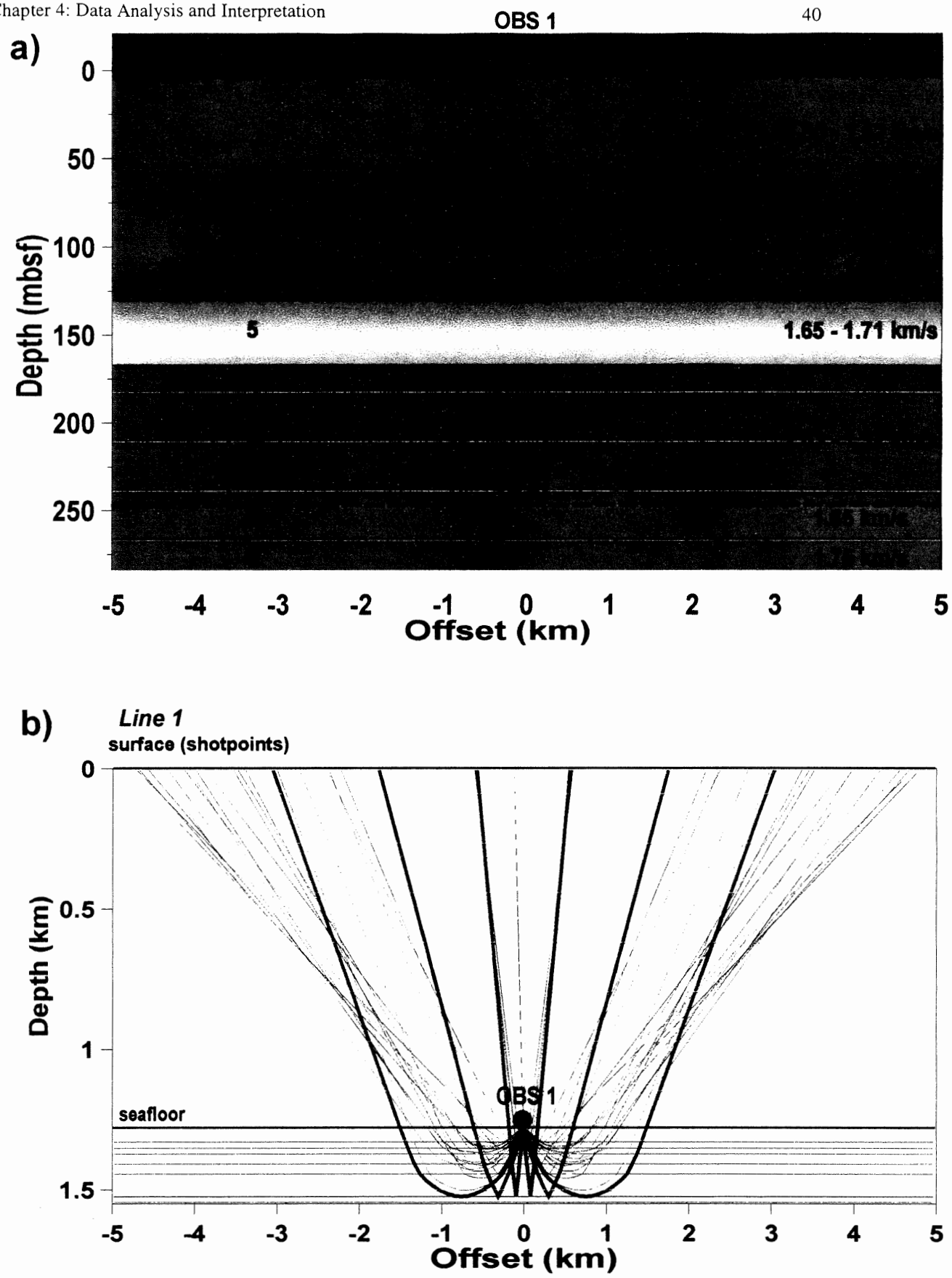

Figure 4.6 a) Velocity-depth 2-D model (assuming homogeneous layers with velocity gradients) (Model 2) showing high velocity lid for methane hydrate zone (1.83 - 1.92 km/s) and a BSR depth of 247 mbsf. b) Raypath display for calculated travel times for Model 2. Raypaths which bend through methane hydrate zone are outlined in pin

layer. Layer 1- Layer 4 show a fairly steady gradient from the seafloor to 128 mbsf (1.5 – 1.63 km/s), with the exception of a shift to a low velocity zone between Layer 3 and Layer 4, followed by a steep gradient in Layer 5 (1.65 – 1.72 km/s), then a large shift in the velocities at approximately 165 mbsf between Layer 5 and Layer 6. Layer 6 ranges from 1.83 km/s at the top to 1.92 km/s at the bottom. The bottom of Layer 6 (BSR) is approximately 247 mbsf. Figure 4.7 displays the travel time curves produced from the fitting of this model in normal moveout corrected time and reduced time on the 40 cu. in. data.

4.3.3 Ray Trace Modelling: Model 3 (300 cu. in. airgun source)

In Model 3, the critical factor in determining the velocity gradients are the refracted (or diving) rays which reach the surface before the direct arrival (Fig. 4.1, Fig. 4.2). In this model, the layer above the BSR is assumed to be consistent with the layer which produces the first refracted arrival (phase velocity ~ 1.71 km/s).

Model 3 consists of five layers to the BSR, not including the water layer (Fig. 4.8). The water layer is assumed to have the same upper and lower velocities and water depth as in Model 2. Layer1 – Layer 4 vary linearly from 1.51 to 1.65 km/s. Layer 5 (above the BSR) varies linearly from 1.69 km/s at the top to 1.712 km/s at the bottom, with the BSR approximated at 215 mbsf. The results of travel time inversion of this model can be seen in Figure 4.9. The first refractor to become a primary arrival has a phase velocity of 1.71 km/s, the second refractor has a phase velocity of 1.65 km/s. These velocities are consistent with the base of Layer 5 and the base of Layer 4 respectively.

Model 3 is a starting point for the modelling of velocity gradients in layers above the BSR, however, this model is not compatible with the 40 cu. in. airgun results (Fig. 4.10). Thus, the model is not an acceptable velocity model for both data sets. Similarly, Model 2 can not be fitted

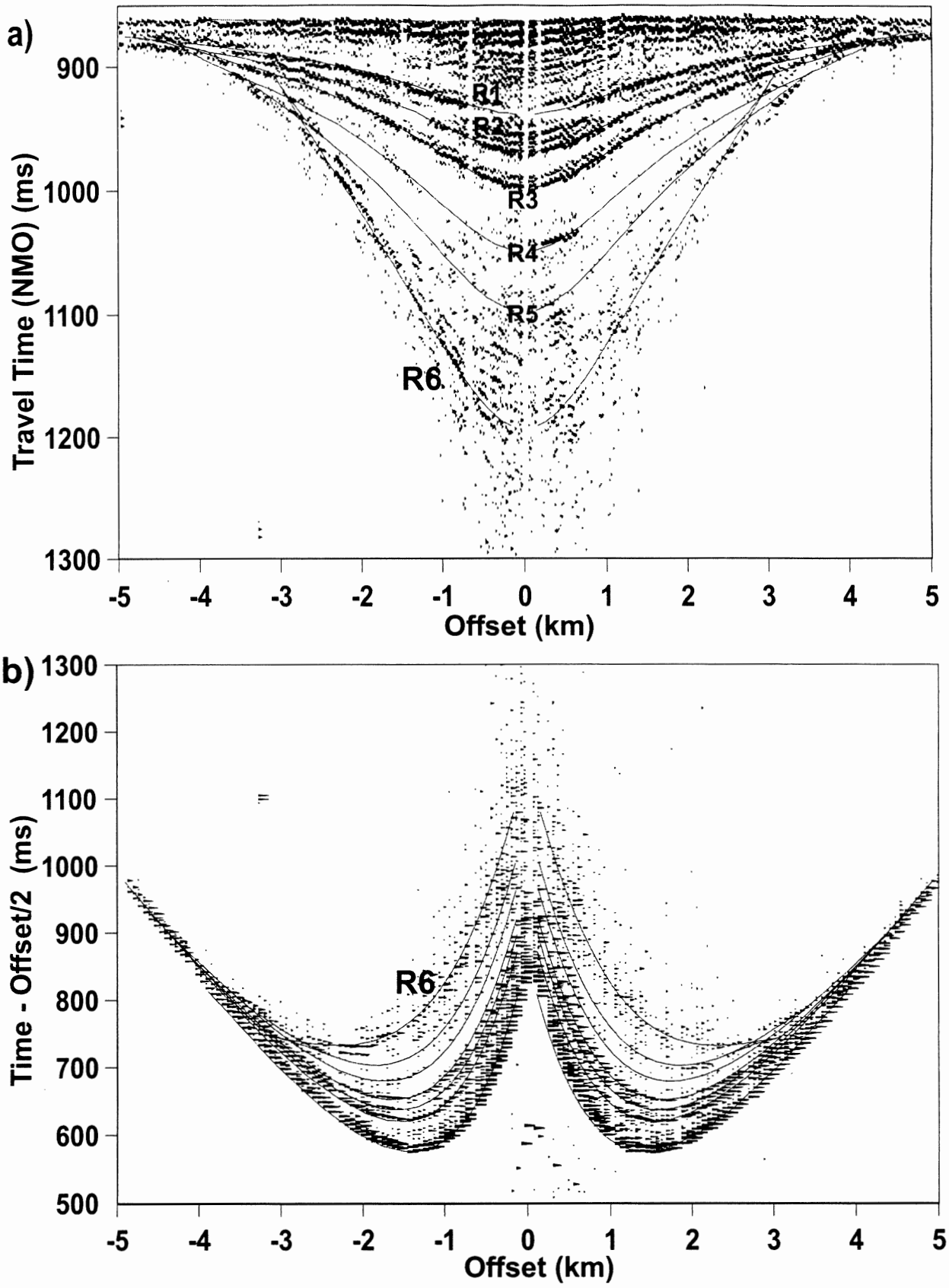

Figure 4.7 Travel time curves fitted by Model 2 overlaying 40 cu. in. airgun data for OBS 1, Line 1 for a) normal moveout correction(1.481 km/s), and b) reduced travel-time plots (2 km/s). Figure 4.7a displays reflectors from the bottom of Layers 1 - 6 (R1 to R6 respectively). R6 represents the modelled BSR.

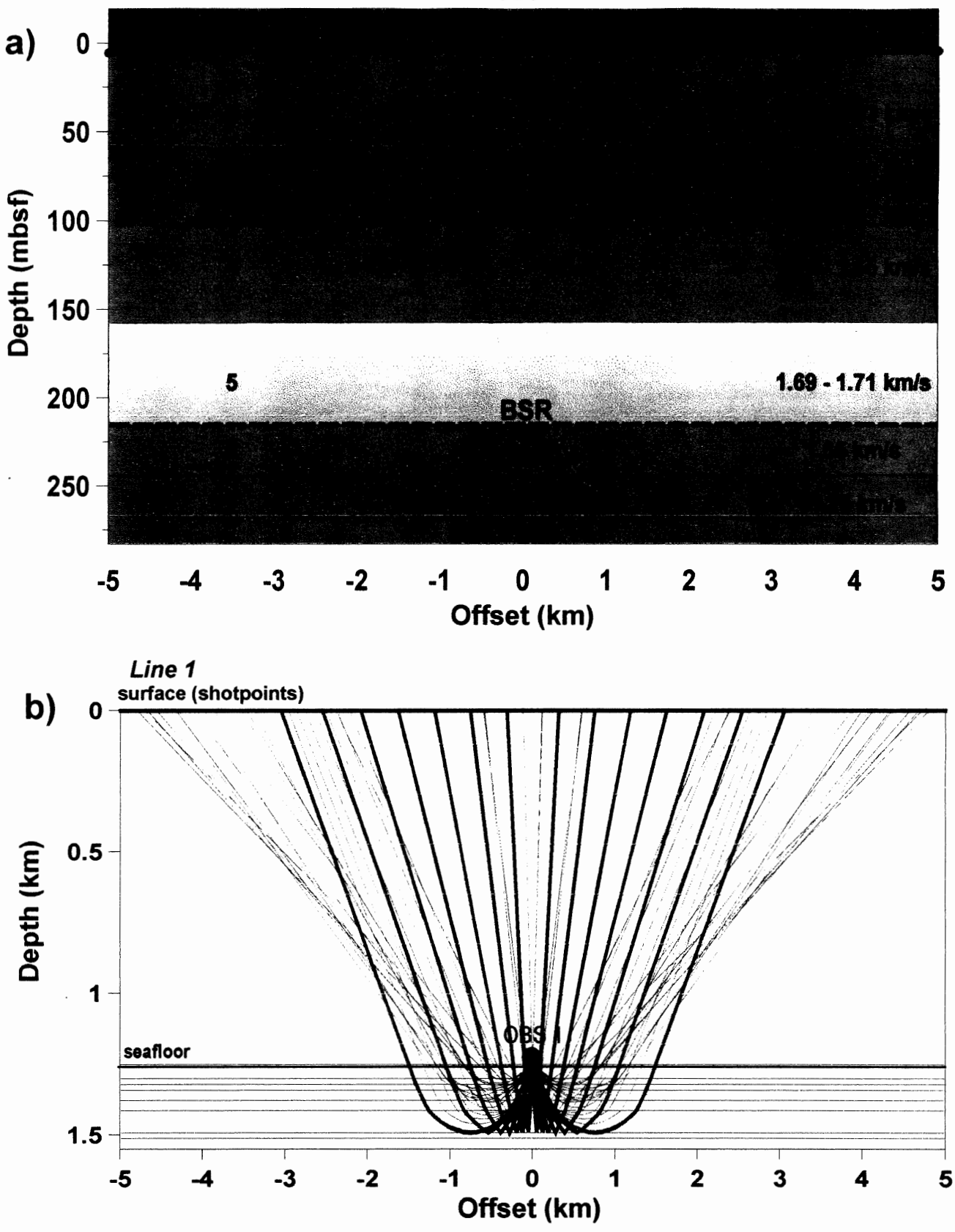

Figure 4.8 a) Velocity-depth 2-D model (assuming homogeneous layers with velocity gradients) (Model 3) showing low velocities for methane hydrate zone (1.69 - 1.71 km/s) and a BSR depth of 215 mbsf. b) Raypath display for calculated travel times for Model 3. Raypaths which bend through methane hydrate zone are outlined in pink.

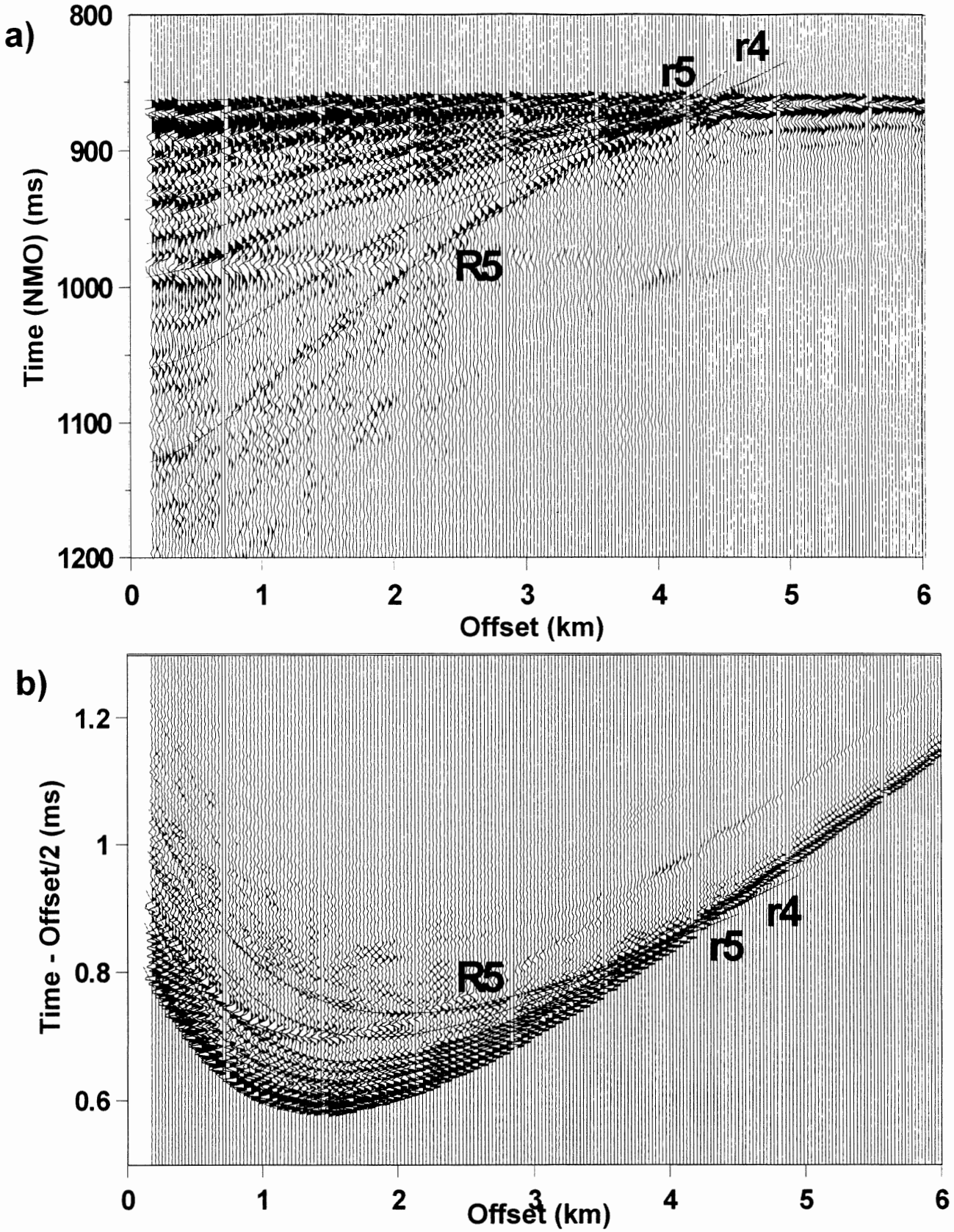

Figure 4.9 Travel time fits for Model 3 plotted on 300 cu. in. airgun source datafor a) normal moveout corrected data, and b) reduced velocity plots. R5 represents reflector from base of Layer 5 (BSR). r5 and r4 are refracted phase arrivals from Layers 5 and 4 respectively. Layer 4 displays velocities of 1.63 km/s and Layer 5 displays velocities of 1.71 km/s.

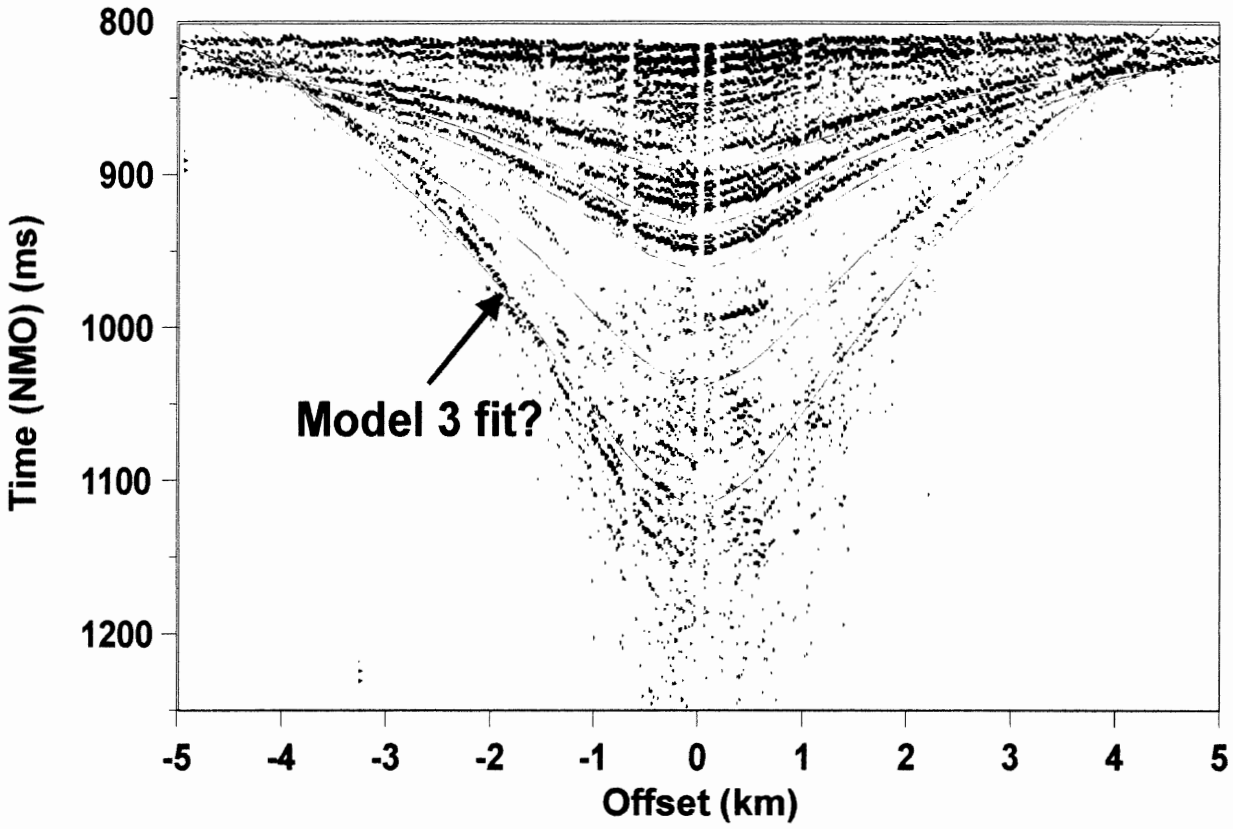

Figure 4.10 Model 3 travel time calculations for five layer model overlaying 40 cu. in. data. This velocity model requires further adjustments in order to fit the travel times of both reflectors and refractors.

to 300 cu. in. airgundata, and must be modified. The final model (Model 4) is produced based on the constraints of these two models.

4.3.4 Final Model: Model 4 (40 cu. in. and 300 cu. in. airgun source)

Model 4 (Fig. 4.11) displays the same general trend in velocity structure as Model 2 and Model 3 for the upper layers, while the two layers above the BSR differ slightly. Six layers are modelled to the depth of the BSR for the 300 cu. in. airgun data. Consistent with Model 3, the second refracted phase arrival is used to determine gradients in Layer 4 (with velocities of 1.64 km/s at the bottom of the layer). Modelling of the first refracted phase arrival from the base of Layer 5 (~1.73 km/s) with the overlying layer gradient is more problematic. The model differs from the previous models in that Layer 5 and Layer 6 contain velocity gradients of 1.69 to 1.73 km/s and 1.79 to 1.86 km/s respectively in a relatively small vertical distance from the BSR (approximately 66 m, as opposed to approximately 120 m for Model 2). The BSR depth is approximately 220 m. Figure 4.12 displays the travel time fits of the Model 4 velocity structure on the normal moveout corrected 40 cu. in. and 300 cu. in. (positive offset) data.

A crucial difference between the previous models and Model 4 is the reflector modelled in Model 4 (Layer 6 – Layer 7 transition), which possibly represents the transition from a low velocity free-gas zone to a less gas-rich sediment. This underlying low velocity - high velocity reflector (1.68 to 1.75 km/s) acts as a strong reflector at relatively low offsets for the 40 cu. in. airgun (~242 mbsf), whereas the overlying high velocity - low velocity reflector (1.86 to 1.68 km/s) is believed to be the stronger BSR visible with the 300 cu. in. airgun source (~220 mbsf). Thickness of this low velocity layer zone is estimated to be approximately 22 +/- 5 m by the fitted travel times, given an assumed free-gas rich sediment of 1.68 km/s (MacKay et al., 1994).

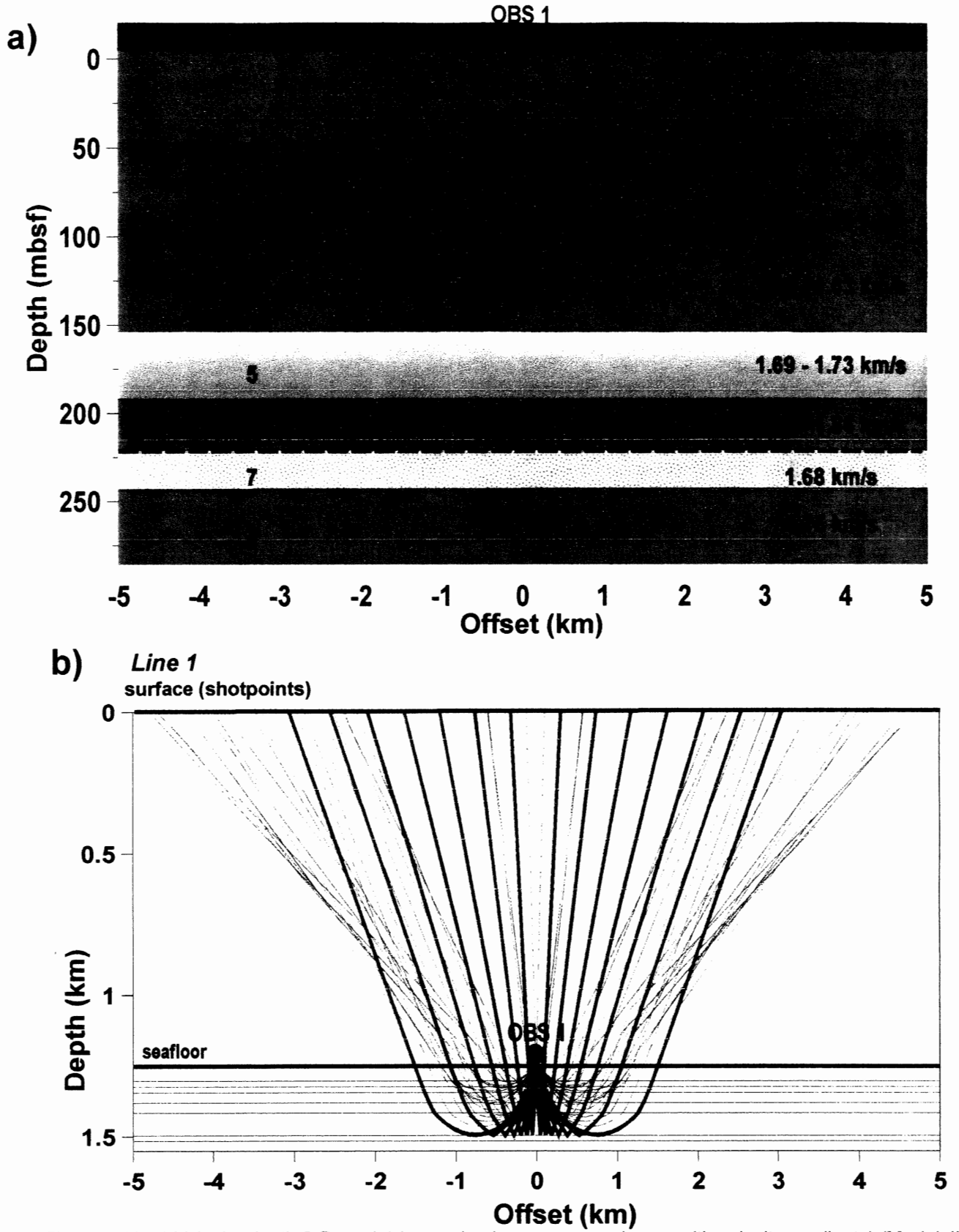

Figure 4.11 a) Velocity-depth 2-D model (assuming homogeneous layers with velocity gradients) (Model 4) showing high velocity lid for methane hydrate zone (1.79 - 1.86 km/s) and a BSR depth of 220 mbsf. b) Raypath display for calculated travel times for Model 4. Raypaths which bend through methane hydrate zone are outlined in pink.

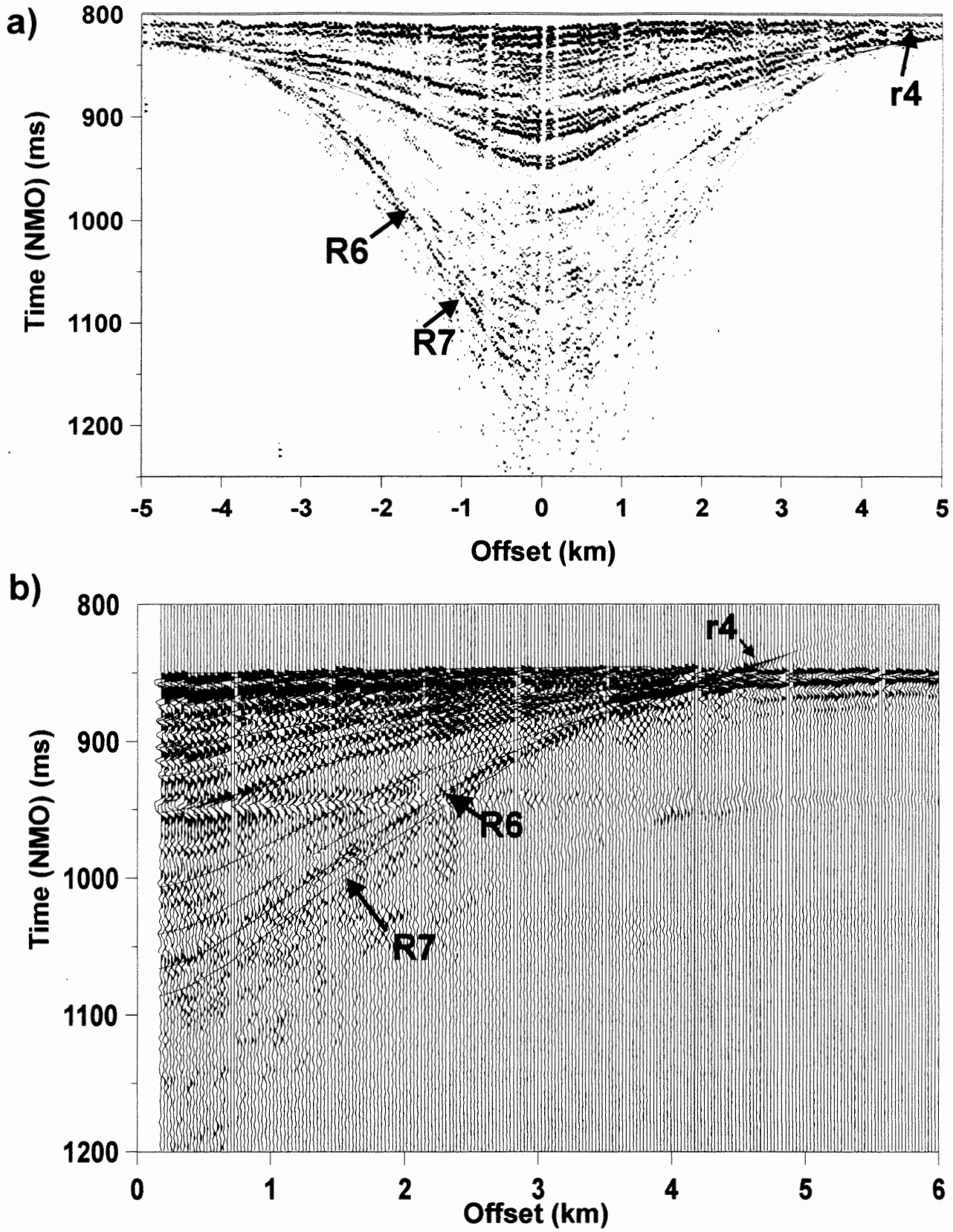

Figure 4.12 Model 4 travel time calculations fitted over normal moveout corrected data for OBS 1, Line 1 for a) 40 cu. in. airgun (positive and negative offsets), and b)300 cu. in. airgun (positive offsets only). R6 is the reflector from the bottom of the high velocity methane hydrate zone layer (BSR). R7 is underlying refector from base of free gas layer. r4 represents refracted phase arrivals from the bottom of Layer 4 (~1.65 km/s).

4.4 Interpretation and Discussion

The most notable interpretation from the models presented thus far for OBS 1, Line 1 is the variance in the BSR with different frequencies for the airgun source. Velocity-depth models based on the 40 cu. in. airgun source suggests a BSR depth of approximately 240 mbsf and relatively high velocities in the methane hydrate stability zone (1.83 – 1.92 km/s). In contrast, velocity-depth model of the 300 cu. in. data suggests a BSR depth of approximately 220 m, with relatively lower velocities occurring in the methane hydrate stability zone (1.69 – 1.72 km/s).

A refined model arises from these differences, which might account for this visible variance in the BSR. The reflector near vertical incidence for the 40 cu. in. airgun source is not interpreted as being representative of a BSR. Instead, there are two separate phases which are interpreted to be apparent with the 40 cu. in. airgun source: 1) a major acoustic impedance (BSR) at the hydrate - free-gas boundary (from 1.86 to 1.68 km/s), which is consistent with the 300 cu. in. airgun profiles, and 2) a separate reflector at the base of the free-gas zone (from 1.68 to 1.75 km/s), where sediment velocities shift to the estimated velocity gradient with depth as a result of compaction, which becomes visible near vertical incidence with the 40 cu. in. airgun source. This final model (Fig 4.13) suggests that hydrate concentrations increase slightly at approximately 66 m above the BSR (transition from 1.69 to 1.73 km/s). A sharp increase in hydrate concentration occurs in a zone approximately 30 m thick (188 – 220 mbsf) above the BSR with velocities of 1.79 to 1.86 km/s. A free gas zone exists below this layer which is approximately 22 m thick with a velocity of 1.68 km/s. This model is consistent with both the reflected phase arrivals from the 40 cu. in. airgun and refracted phase arrivals from the 300 cu. in. data.

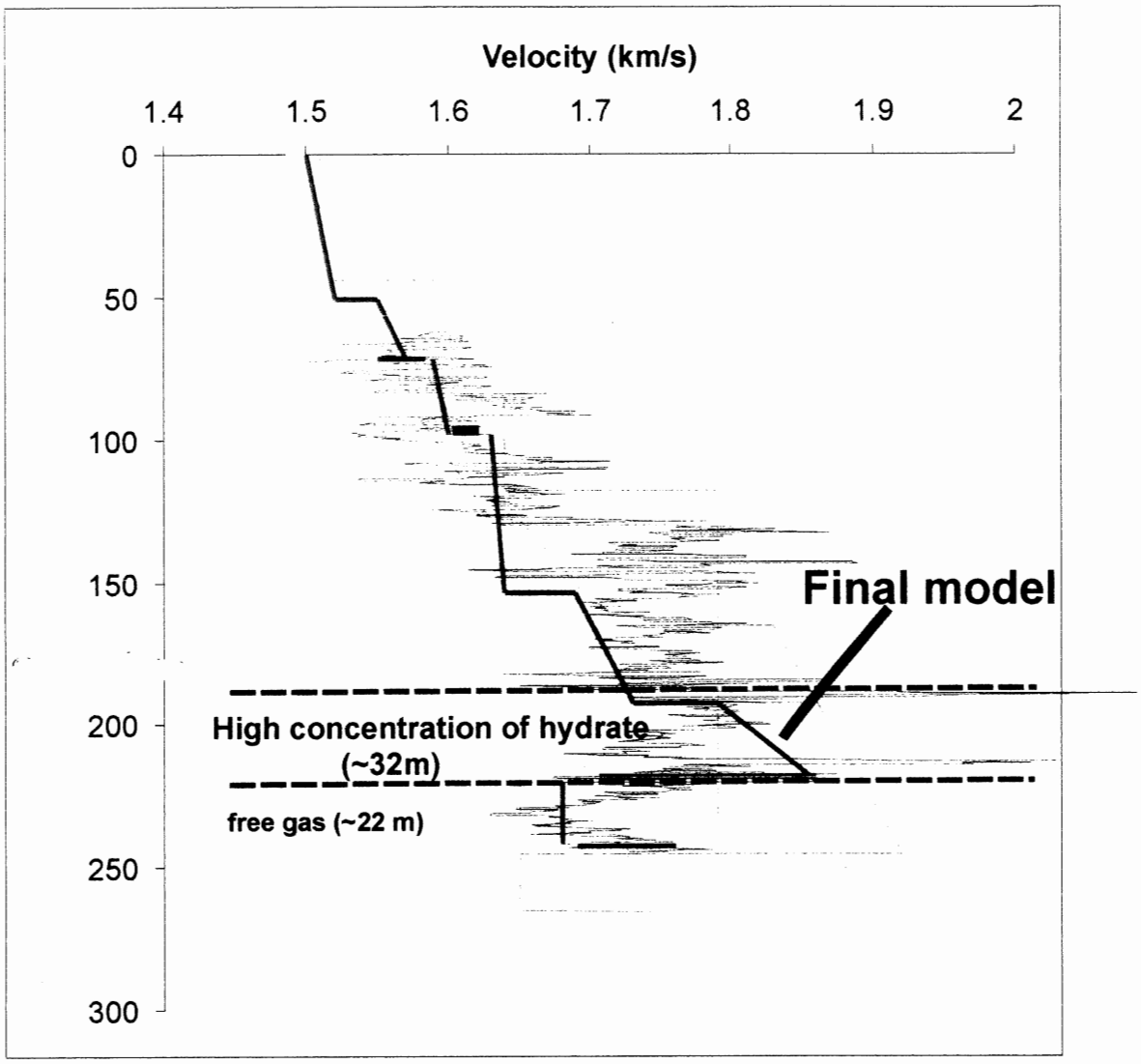

Figure 4.13. Models 1-4 are displayed over sonic log data from ODP Site 889 (Model 1 - pink, Model 2 - brown, Model 3 - green, and Model 4 - thick red). The final model indicates rather low velocity gradients with depth, then a rapid shift at approximately 190 m to a high velocity zone (1.79 - 1.86 km/s) with a relatively highgradient above the BSR. BSR depth for the final model is estimated at 220 mbsf. The existence of a free gas layer is estimated to be 22 m thick.

Based on this evidence, the BSR is likely the result of a high velocity "lid" which accounts for the high impedance contrast. Nevertheless, the seismic characterization of this high-low velocity contrast is not as clearly observable at vertical incidence for higher frequency sources (40 cu. in. airgun ~ 150 Hz) as it is for lower frequency sources (300 cu. in. airgun ~30 Hz), suggesting some degree of frequency dependence on the nature of the BSR. These gaps in the BSR have been observed by Spence et al. (1994) as most evident with smaller airgun sizes (eg. 40 cu. in.), and are likely the result of higher frequency signals being affected by small-scale lateral variations in structure producing frequency dependent scattering. Some degree of frequency dependence on the resolution of the BSR does appear to be consistent with the data in this case. This variation could be better resolved by horizontal ray trace modelling as well as vertical modelling (1-D) of the velocity transitions, which is not covered in the scope of this project.

The proposed gradation of hydrate from the seafloor to the base of the hydrate stability zone seems unlikely from these analyses. A sharp increase in the velocity (1.73 - 1.79 km/s) approximately 32 m to a zone above the BSR inferred from this model is consistent with various gradational velocity-models proposed for the Cascadia Margin methane hydrate fields (Hyndman and Spence, 1992; Hyndman, 1995). However, the results from this study show the zone above the BSR to be significantly thinner than these other models (eg. ~100 m thickness), and with sharper velocity gradient. Based on the formulas given by Yuan et al. (1996) (Eqn. 2.1), estimated hydrate concentration levels are on the order of 15 to 20 % of pore space (Fig.2.2).

Evidence from these ray tracing models of a low velocity free-gas zone below the BSR is consistent with in situ drilling results from ODP Site 889, as well as the full waveform inversion analyses of Singh and Minshull (1994). The inferred P-wave velocities of the sediments from drilling results below the BSR suggest that 2 - 3% free gas exists (Westbrook et al., 1994), creating

anomalously low velocities (~1.4 - 1.65 km/s), which result in a strong impedance contrast. Drilling results are limited to a depth of 15 m below the BSR, suggesting a free gas zone of at least 15 m thick. However, Singh and Minshull (1994) also propose that the velocity transition below the BSR is gradational back to high velocities and is approximately 30 m thick. Based on the analyses presented here, a partially saturated free gas zone is proposed to exist which is approximately 22 m thick. Gradation to higher velocities seems unlikely given that a strong reflector appears from the base of this free-gas zone, as seen in the Blake-Bahama ridge methane hydrate gas fields (eg. Katzman and Holbrook, 1994; Miller et al., 1991).

4.5 Future Work

This project has presented seismic data located on a ridge structure of the accretionary prism of the Cascadia Margin, which is essentially the first half of an entire project. Futher research of the methane hydrate zone in the basin structures would involve the analysis of data from OBS 4, 5, and 6. Integration of data from various OBSs would also be required to better model the velocity-depth structure of the area. The fulfillment of this entire project would then lead to a better understanding of the continuity of methane hydrates within zones with a strong BSR and areas of a discontinuous BSR. Future work also includes: 1) synthetic seismograms produced from the velocity-depth models to compare with actual amplitude data, 2) an amplitude vs. offset analysis, in order to fully understand the continuity of the reflection, 3) and applying Zelt's method for travel-time inversions, given a starting velocity model.

CHAPTER 5 CONCLUSIONS

In summary, the following conclusions are interpreted from the results of wide-angle seismic reflected and refracted arrivals of OBS 1, Line 1:

1. Wide-angle reflection and refraction arrivals from 40 cu. in. airgun sources and 300 cu. in. airgun sources display variability in the strength of the BSR at vertical incidence. The higher frequency source (40 cu. in.) displays a weaker BSR at vertical incidence than that of the lower frequency source (300 cu. in.). This effect is interpreted to be the result of frequency scattering due to lateral variation in the continuity of the free gas beneath the phase transition of methane hydrate and free methane gas.

2. Refracted phase arrivals visible with the 300 cu. in. airgun source represent velocity gradients of layers above the methane hydrate stability zone (~ 1.65 - 1.71 km/s). The gradient of the methane hydrate zone is relatively sharp, as refracted phase arrivals consistent with velocities of hydrated sediments are not visible in these profiles, and the raypaths do not reach great offsets.

3. The raytracing method for one dimensional velocity-depth modelling was applied successfully to fit wide-angle data for both 40 cu. in. and 300 cu. in. airgun sources. The depth to the BSR is consistent with previous documented results (~220 m). The model indicates velocities directly above the BSR range from 1.79 to 1.86 km/s in a zone approximately 32 km thick. These values suggest that estimated hydrate concentrations of 15 - 20 % occur in the pore spaces of this zone, and increase significantly directly above the BSR.

4. The existence of a free gas zone approximately 22 m thick (*P*- wave velocities ~ 1.65 km/s) is proposed to exist below the high velocity zone (beneath the BSR). A

significant phase transition from this free gas layer to higher velocities below the BSR is evident on the lower frequency airgun source (40 cu. in.), whereas only the BSR can be identified from the 300 cu. in. airgun sources.

References

Brooks, J.M., Anderson, A.L., Sassen, R., MacDonald, I.R., II, M.C.K., and Guinasso, N.L., 1994. Hydrate occurrences in shallow subsurface cores from continental slope sediments. In *International conference on natural gas hydrates.* Sloan, E.D., Happle, J., and Hnatow M.A., (Eds.), vol. 715, Plenum Press, New York. pp.381-391.

Claypool, G.E., and Kaplan, I.R., 1974. The origin and distribution of methane in marine sediments, in *Natural Gases in Marine Sediments,* edited by I.R. Kaplan. Plenum, New York. pp. 99-140.

Davis, E.E., and Hyndman, R.D., 1989. Accretion and recent deformation of sediments along the northern Cascadia subduction zone. *Geol. Soc. Am. Bull.,* **101**:1465-1480.

DeMets, C., Gordon, R.G., Argus, D.F., and Stein, S., 1990. Current plate motions, *Geophys. J. Int.,* **101**:425-478.

Duncan, R.A., and Kulm, L.D., 1989. Plate tectonic evolution of the Cascades subduction complex. *In* Winterer, E.L., Hussong, D.M., and Decker, R.W. (Eds.), *The Eastern Pacific Ocean and Hawaii.* Geol. Soc. Am.,413-438.

Hesse, R., 1986. Diagenesis #11: early diagenetic pore water/sediment interaction:modern offshore basins. *Geoscience Canada,* **14**:165-195.

Howell, D.G., Jones, D.L., and Schermer, E.R., 1985. Tectonostratigraphic terranes of the circum-Pacific region. *In PreliminaryTectonostratigraphic Terrane Map of the Circum-Pacific Region.* AAPG.

Hyndman, 1995.The Lithoprobe corridor across the Vancouver Island continental margin: the structural a and tectonic consequences of subduction. *Can. J. Earth. Sci.* **32:** 1777 - 1802 .

Hyndman, R.D., and Davis, E.E., 1992. A mechanism for the formation of of methane hydrate and sea floor bottom simulating reflectors by vertical fluid expulsion. *J. Geophys. Res.*, **97**: 7025 - 7041.

Hyndman, R.D., and Spence, G.D., 1992. A seismic study of methane hydrate marine bottom simulating reflectors. *J. Geophys. Res.*, **97**:6683-6698.

Hyndman, R.D., Foucher, J.P., Yamano, M., et al., 1992. Deep sea bottom-simulating reflectors: calibration of the base of the hydrate stability field as used for heat flow measurements. *Earth Planet. Sci. Lett.*, **109**:289-302.

Katzman, R., and Holbrook, W.S., 1994. Combined vertical incidence and wide - angle study of a gas hydrate zone, Blake Ridge. *J. Geophys.l Res..*, **99**: 17975 - 17 995.

Katzman, R., Holbrook, W.S., and Paull, C.K., 1994. Combined vertical incidence and wide-angle seismic study of a gas hydrate zone, Blake Ridge. *J. Geophys.Res.* **99**:17975-17995.

Korenaga, J., Holbrook, W.S., Singh, S.C., and Minshull, T.A., 1997. Natural gas hydrates on the southeast U.S. margin: Constraints from full waveform and travel time inversions of wide-angle seismic data. *J. Geophys. Res.* **102**:345-365.

Kvenvolden, K.A., 1988. Methane hydrate - a major reservoir of carbon in the shallow geosphere ? Chemical Geology, **71**:41-51.

Kvenvolden, K.A., 1993. Gas hydrates-geologic perspective and global change. *Rev.Geophys.* **31**:173-187.

Kvenvolden, K.A., Claypool, G.E., Threkeld, C.N., and Sloan, E.D., 1984. Geochemistry of a naturally occurring massive marine gas hydrate. *Org. Geochem.,* **6**:703-713.

Lee, M.W., Hutchinson, D.R., Dillon, W.P., Miller, J.J., Agena, W.F., and Swift, B.A., 1994. Seismic character of gas hydrates on the southeastern U.S. continental margin. *Mar. Geophys. Res.* **16**:163-184.

MacDonald, G.J., 1990. Role of methane clathrates in past and future climates. Climatic Change, **16**:247 - 281.

MacKay, M.E., Jarrard, R.D., Westbrook, G.K., Hyndman, R.D., and the Shipboard Scientific Party of ODP Leg 146, 1994. Origin of bottom simulating reflectors: Geophysical evidence from the Cascadia accretionary prism. *Geology*, **22**:459-462.

Miller, J.J., Lee, M.W., and von Heune. R., 1991. A quantitative analysis of gas hydrate phase boundary reflection (BSR), offshore Peru. American Association of Petroleum Geologists Bulletin, 75: 910 - 924.

Monger, J.W.H., Price, R.A., and Tempelman-Kluit, D.J., 1982. Tectonic accretion and the origin of the two major metamorphic and plutonic welts in the Canadian Cordillera. *Geology*, 10:7075.

Paull, C.K., Ussler, w., and Borowski, W.S, 1994. *Sources of biogenic methane to form marine gas*

hydrates. In *International conference on natural gas hydrates.* Sloan, E.D., Happle, J., and Hnatow, M.A., (Eds.), vol.715, Plenum Press, New York, pp. 393-409.

Riddihough, R.P., 1984. Recent movements of the Juan de Fuca Plate system. *J. Geophys. Res.,* **89**:6980-6994.

Rowe, M.M., and Gettrust, J.F., 1994. Methane hydrate content of Blake Outer Ridge sediments. In *International conference on natural gas hydrates.* Sloan, E.D., Happle, J., and Hnatow M.A., Eds., vol. 715, Plenum Press, New York. pp.381-391.

Shipley, T.H., Houston, M.H., Buffler R.T., et al., 1979. Seismic evidence for widespread possible gas hydrate horizons on continental slopes and rises. American Association of Petroleum Geologists Bulletin, **63**: 2204 - 2213.

Singh, S.C. and Minshull, T.A., 1994. Velocity structure of a gas hydrate reflector at Ocean Drilling Program site 889 from global seismic waveform inversion. *J. Geophys. Res.,* 99:24,221-224,233.

Sloan, E.D., 1990. *Clathrate hydrates of natural gases.* Marcel Bekker Inc., New York, pp. 1-641.

Spence. G.D., Hyndman, R.D., et al., 1991. Seismic structure of the northern Cascadia accretionary prism: evidence from new multichannel seismic reflection data. *In* Meissner, R., Brown, L., Birbaiet, W., Franke, K., Fuchs, K., and Seifert, F. (Eds.), *Continental Lithosphere, Deep Seismic Reflection.* Am. Geophys. Union. Geodyn. Ser., **22**:257-263.

Spence, G.D., Minshull, T.A., and Fink, C., 1995. Seismic studies of methane gas hydrate, offshore Vancouver Island. In *Proc. of Ocea. Drill. Prog., Sci. Results.* Vol. 146. (Pt. 1) Carson, B., Westbrook, G.K., Musgrave, R.J., and Suess, E. (Eds.). College Station, TX (Ocean Drilling Program).

von Huene, R., and Kulm, L.D., 1973. Tectonic summary of Leg 18. *In* Kulm, L.D., von Huene, R., et al., *Init. Repts. DSDP:* Washington (U.S. Govt. Printing Office), 961-976.

von Huene, R. et al., 1985. *Initial Rep. Deep Sea Drill Proj.,* vol. 84. U.S. Printing Office, Washington, D.C., 1985, pp. 1-967.

Westbrook, G.K., Carson, B., Musgrave, R.J. et al., 1994. Proceedings of the Ocean Drilling Program, Initial reports, **146** (Part 1), College Station, TX (Ocean Drilling Program).

Whalley, E., 1980. Speed of longitudinal sound in clathrate hydrates. *J. Geophys. Res.* **85**: 2539-2542.

Yorath, C.J., 1987. Petroleum geology of the Canadian Pacific continental margin. *In* Scholl, D.W., Grantz, A., and Vedder, J.G. (Eds.), *Geology and Resource Potential of the Continental Margin of Western North America and Adjacent Ocean Basins-Beaufort sea to Baja California.* Circum-Pac. Counc. Energy Miner. Resourc., 283-304.

Yuan, T., Spence, G.D., and Hyndman, R.D., 1994. Seismic velocities and inferred porosities in the accretionary wedge sediments at the Cascadia Margin. *J. Geophys. Res.,* **99**:4413-4427.

Yuan, T., Hyndman, R.D., Spence,G.D., and Desmons, B., 1996. Seismic velocity increase and deep-sea gas hydrate concentration above a bottom-simulating reflector on the northern Cascadia continental slope. *J. Geophys. Res.,* **101**:13655-13671.

Zelt, C.A., and Smith, R.B., 1992. Seismic traveltime inversion for 2-D crustal velocity structure. *Geophys. J. Int.,* **108**:16-34.